NSWC TR 88-292

OBSERVATIONS ON THE INFLATION TIME AND INFLATION DISTANCE OF PARACHUTES

BY WILLIAM P. LUDTKE

UNDERWATER SYSTEMS DEPARTMENT

28 MAY 1988

NAVAL SURFACE WARFARE CENTER
Dahlgren, Virginia 22448-5000 • Silver Spring, Maryland 20903-5000

REPORT DOCUMENTATION PAGE

1a. REPORT SECURITY CLASSIFICATION UNCLASSIFIED	1b. RESTRICTIVE MARKINGS
2a. SECURITY CLASSIFICATION AUTHORITY	3. DISTRIBUTION/AVAILABILITY OF REPORT Approved for public release Distribution unlimited
2b. DECLASSIFICATION/DOWNGRADING SCHEDULE	
4. PERFORMING ORGANIZATION REPORT NUMBER(S) NSWC TR 88-292	5. MONITORING ORGANIZATION REPORT NUMBER(S)
6a. NAME OF PERFORMING ORGANIZATION Naval Surface Warfare Center White Oak, Silver Spring, MD 6b. OFFICE SYMBOL (If applicable) U13	7a. NAME OF MONITORING ORGANIZATION
6c. ADDRESS (City, State, and ZIP Code) 10901 New Hampshire Ave. Silver Spring, MD 20903-5000	7b. ADDRESS (City, State, and ZIP Code)
8a. NAME OF FUNDING/SPONSORING ORGANIZATION 8b. OFFICE SYMBOL (If applicable)	9. PROCUREMENT INSTRUMENT IDENTIFICATION NUMBER
8c. ADDRESS (City, State, and ZIP Code)	10. SOURCE OF FUNDING NUMBERS PROGRAM ELEMENT NO.: NA PROJECT NO.: 9U91VB TASK NO.: NA WORK UNIT ACCESSION NO.: NA

11. TITLE (Include Security Classification)
Observations on the Inflation Time and Inflation Distance of Parachutes

12. PERSONAL AUTHOR(S)
WILLIAM P. LUDTKE

13a. TYPE OF REPORT	13b. TIME COVERED	14. DATE OF REPORT (Year, Month, Day)	15. PAGE COUNT
Final	FROM FY'88 TO FY'89	5-28-88	82

16. SUPPLEMENTARY NOTATION

17. COSATI CODES			18. SUBJECT TERMS (Continue on reverse if necessary and identify by block number)
FIELD	GROUP	SUB-GROUP	Parachute Technology; Calculation Methods; Inflation Time; Inflation Geometry; Inflation Distance; Solid Cloth Parachutes
01	03		

19. ABSTRACT (Continue on reverse if necessary and identify by block number)

This report summarizes the comments on parachute inflation time and distance from several of the author's previous publications. Additional information is included to explain how recovery systems opening shock forces are determined not only by the specified operational velocity, altitude, and trajectory angle, but are also determined by the initial program requirements of weight, rate of descent, equilibrium altitude, choice of parachute type, and canopy airflow.

Two accepted axioms on the constancy of inflation distance and the effect of inflation time on the magnitude of the opening shock force are analyzed. The results verify that the inflation distance axiom is correct, and that the inflation time-opening shock axiom is not correct although it appears to be.

20. DISTRIBUTION/AVAILABILITY OF ABSTRACT	21. ABSTRACT SECURITY CLASSIFICATION	
☐ UNCLASSIFIED/UNLIMITED ☒ SAME AS RPT. ☐ DTIC USERS	UNCLASSIFIED	
22a. NAME OF RESPONSIBLE INDIVIDUAL WILLIAM P. LUDTKE	22b. TELEPHONE (Include Area Code) (202) 394-1075	22c. OFFICE SYMBOL U13

DD FORM 1473, 84 MAR 83 APR edition may be used until exhausted.
All other editions are obsolete

SECURITY CLASSIFICATION OF THIS PAGE

☆ U.S. Government Printing Office: 1986—607-044

FOREWORD

This report summarizes the comments on parachute inflation time and distance from several of the author's previous publications. Additional information is included to explain how recovery systems opening shock forces are determined not only by the specified operational velocity, altitude, and trajectory angle, but are also determined by the initial program requirements of weight, rate of descent, equilibrium altitude, choice of parachute type, and canopy airflow.

Two accepted axioms on the constancy of inflation distance and the effect of inflation time on the magnitude of the opening shock force are analyzed. The results verify that the inflation distance axiom is correct, and that the inflation time-opening shock axiom is not correct although it appears to be.

W. W. Wassmann

W. W. WASSMANN, Head
Underwater Weapons Division

CONTENTS

ILLUSTRATIONS

ILLUSTRATIONS (Cont.)

TABLES

INTRODUCTION

One important aspect of parachute technology is the determination of the opening shock force under specified operational conditions. Two often heard common axioms, concerning the parachute deployment process, are:

AXIOM 1: The product of the system velocity at suspension line stretch and the inflation time is a constant inflation distance.

AXIOM 2: Parachute opening shock force is a strong function of inflation time.

The inflation distance of axiom one is presently determined experimentally from field test data. The graphing of opening shock forces versus inflation time certainly presents a picture that strongly supports axiom two. What is needed is a theoretical analysis which can make clear the relationship of the two axioms to the retardation system design requirements, operational altitude and velocity, trajectory deployment angle, type of parachute, and airflow through the canopy.

A method of calculating the inflation reference time and distance of solid cloth parachutes was developed and shows that a parachute system's performance is not determined solely by the specified operational altitude and velocity. It is more fundamental than that. Rather a system's performance is also determined when the basic parachute system requirements; i.e., rate of descent and altitude, system weight to be recovered, type of parachute, and canopy cloth are selected.

It should be obvious that the inflation effects depend on the basic system requirements as well as the operational requirements. Sometimes I have the feeling that designers treat the basic requirements as a separate and independent set of calculations from the deployment effects and that the "system performance" is limited to application of the operational altitude, velocity, and trajectory angle.

This report treats the development and examination of the inflation distance and reference time of parachutes. It is a composite of the individual observations from the several references with additional development and comments to demonstrate that axiom one is true and that axiom two appears to be true, but really is not.

APPROACH

The inflation of any parachute is a very complicated process. During the inflation time period the mouth area, pressurized canopy surface area, and parachute drag area are varying. The instantaneous rate of airflow into the canopy mouth and out through the transient pressurized canopy area are changing. Also, the velocity profile during inflation, Reference 1,which affects the canopy rate of airflow and the inflation reference time, is dependent upon the system weight, operational altitude, parachute size, and trajectory angle, Reference 2. Under certain conditions of canopy airflow and altitude, the parachute may partially inflate. The progression of the inflation process is a function of:

a. Type of parachute

b. Weight to be recovered, including the weight of the parachute

c. Parachute drag area

d. Canopy rate of airflow

e. Operational altitude

f. Instantaneous trajectory velocity

The calculation of the inflation reference time is required for particular solutions to opening shock problems. Methods using the listed criteria in a basic force analysis are developed in References 3, 4, and 5. Any meaningful analysis of inflation forces, inflation reference time, and distance must include the stated effects, as well as produce the effects that have been observed in the field.

DEVELOPMENT OF THE INFLATION TIME AND DISTANCE EQUATIONS

The nomenclature of the various parameters to be discussed is presented on Page 16 of Appendix A. (See Appendix B as a guide for the use of Appendix A.)

The referenced opening shock force studies used ratios of drag area, velocity and time to determine the shock factors, and the time of occurrence of maximum shock force during the inflation process. The ratio concept is an ideal method to analyze the effects of the various parameters on the velocity and force profiles of the opening parachutes; however, a means of calculating the inflation reference time t_o is required before specific values can be computed. Methods for computing the varying mass flow into the inflating canopy mouth, the varying mass flow out through the varying inflated canopy surface area, and the volume of air, $\underline{V}_o$, which must be collected during the inflation process are required.

The mass of air flowing into the canopy mouth, m inflow, has the velocity reduced which raises the canopy internal pressure. This pressure differential relative to the canopy cloth causes some of the air to escape through the canopy surface, m outflow, from the confinement of the canopy. The rate of outflow is determined by the weave of the cloth for solid cloth canopies or the ribbon grid spacing for geometrically porous canopies and the pressure differential. Excessive rates of airflow result in partially inflated or "squidded" parachutes. This is usually considered as a situation to be avoided. A meaningful inflation analysis must account for the possibility of squidding. The mass of air retained within the canopy, dm, is the difference between the inflow mass and the outflow mass.

$$dm = m\ \text{inflow} - m\ \text{outflow}$$

$$\rho \frac{dV}{dt} = \rho V A_M - \rho P A_S \qquad (1)$$

The solution of Equation (1) consists of three steps. The first step is to find a method of expressing the transient mouth area, A_M, and transient pressurized canopy area, A_S, as a function of the deployment time ratio. Sections I and II of Appendix A describe a method where infinite mass wind tunnel deployments of several types of parachutes were used to determine a dynamic drag area ratio for use in opening shock analysis. A conclusion derived from the dynamic drag area ratio was that the geometry of an inflating parachute was independent of altitude and velocity. Berndt and DeWeese, Reference 6, tested finite mass man carrying parachutes at various altitudes and velocities and had the same results. Their data, Figure 1, was plotted as the ratio of canopy projected area, to surface area S_P/S_0, versus t/t_f. Some very important conclusions can be drawn:

1. The geometry of an inflating parachute is independent of altitude, velocity, and system mass.

2. Since one study demonstrated the independence of drag area and another demonstrated the independence of the projected area to surface area ratio, ALL of the transient geometric shapes of inflating parachutes are repeatable and are also independent of altitude, velocity, and system mass restraints.

3. Since the inflating geometry is repeatable, the transient volume of air that is collected is also repeatable.

Figure 2 represents a solid cloth type parachute canopy at some instant during inflation. At any given instant, the parachute drag area is proportional to the maximum inflated diameter. Also, the maximum diameter in conjunction with the suspension lines determines the inflow mouth area (A-A) and the pressurized canopy area (B-B-B). This observation provided the basis for the following assumptions. The actual canopy shape is of minor importance.

a. The ratio of the instantaneous mouth inlet area to the steady-state mouth area is in the same ratio as the instantaneous drag area. The mouth area is not necessarily circular, but is usually an irregular shape.

$$\frac{A_M}{A_{MO}} = \frac{C_D S}{C_D S_O} \qquad (2)$$

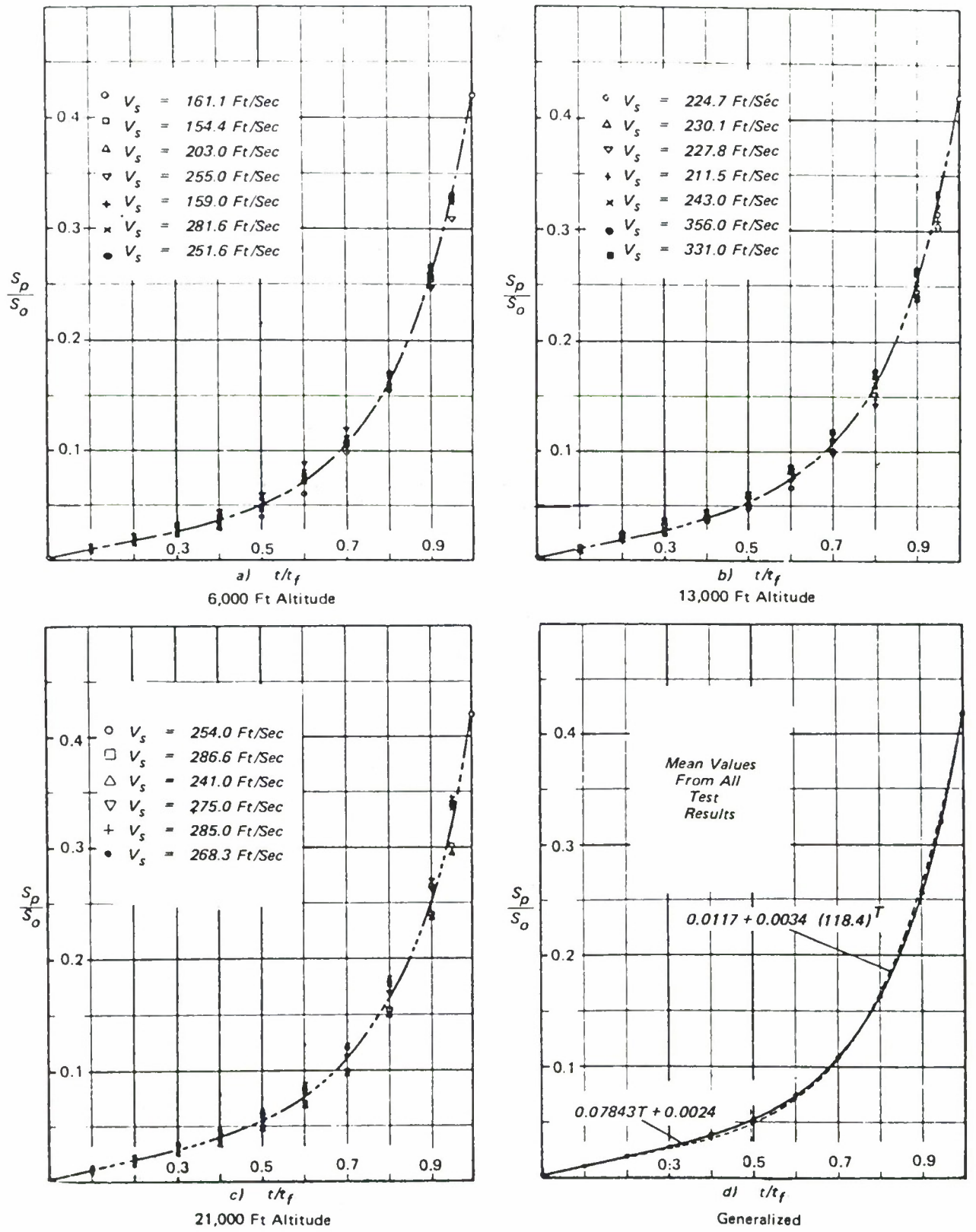

Reproduced from reference 6, page 245

FIGURE 1. NORMALIZED CANOPY AREA GROWTH DURING INFLATION OF 28-FOOT (D_O) SOLID FLAT CIRCULAR PARACHUTE

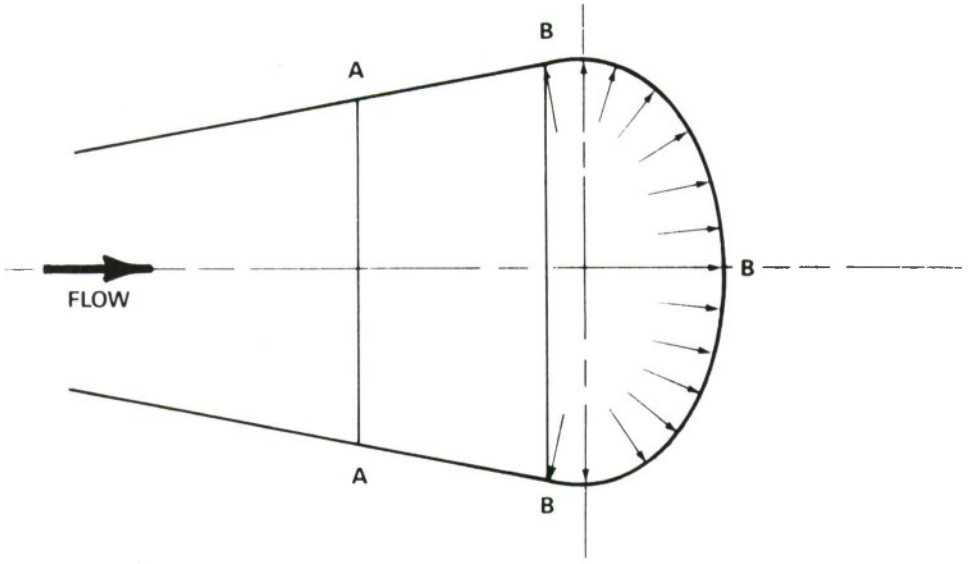

FIGURE 2. PARTIALLY INFLATED PARACHUTE CANOPY

b. The ratio of the instantaneous pressurized cloth surface area to the canopy surface area is in the same ratio as the instantaneous drag area.

$$\frac{S}{S_O} = \frac{C_D S}{C_D S_O} \tag{3}$$

c. Since the suspension lines in the unpressurized area of the canopy are straight, a pressure differential has not developed, and therefore, the net airflow in this zone is zero.

Figure 3 illustrates a typical solid cloth parachute wind tunnel infinite mass force-time history after snatch. In infinite mass deployment, the maximum size and maximum shock force occur at the time of full inflation, t_f. However, t_f is inappropriate for analysis since it is dependent upon the applied load, structural strength, and materials elasticity. The reference time, to, where the parachute has attained its steady-state aerodynamic size, $C_D S_O$, for the first time, is used as the basis for performance calculations.

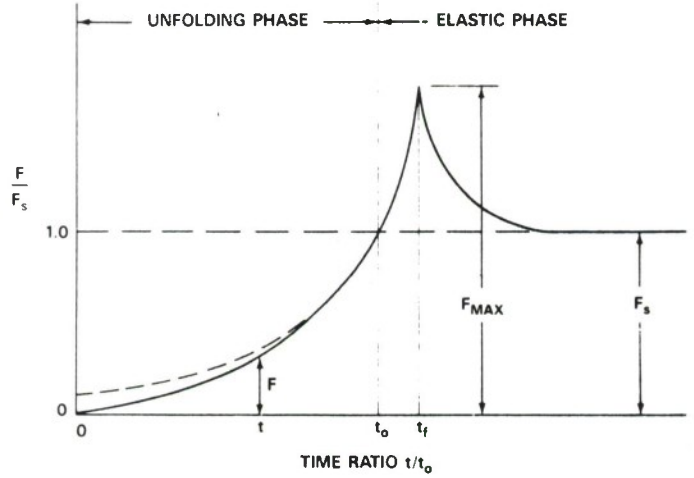

FIGURE 3. TYPICAL INFINITE MASS FORCE-TIME HISTORY OF A SOLID CLOTH PARACHUTE IN A WIND TUNNEL

Infinite mass opening-shock signatures of several types of parachutes are presented in Figures 2 through 6 in Appendix A. Analysis of these signatures using the force ratio, F/F_S versus time ratio, t/t_o, technique indicated a similarity in the performance of the various solid cloth types of parachutes which were examined. The geometrically porous ring slot parachute displayed a completely different signature, as was expected. These data are illustrated in Figure 4. If an initial boundary condition of $C_DS_i/C_DS_O = 0$ at time $t = 0$ is assumed, then, the data can be approximated by fitting a curve of the form.

$$\frac{C_DS}{C_DS_O} = \left(\frac{t}{t_O}\right)^6 \qquad ; \eta = \tau = 0 \tag{4}$$

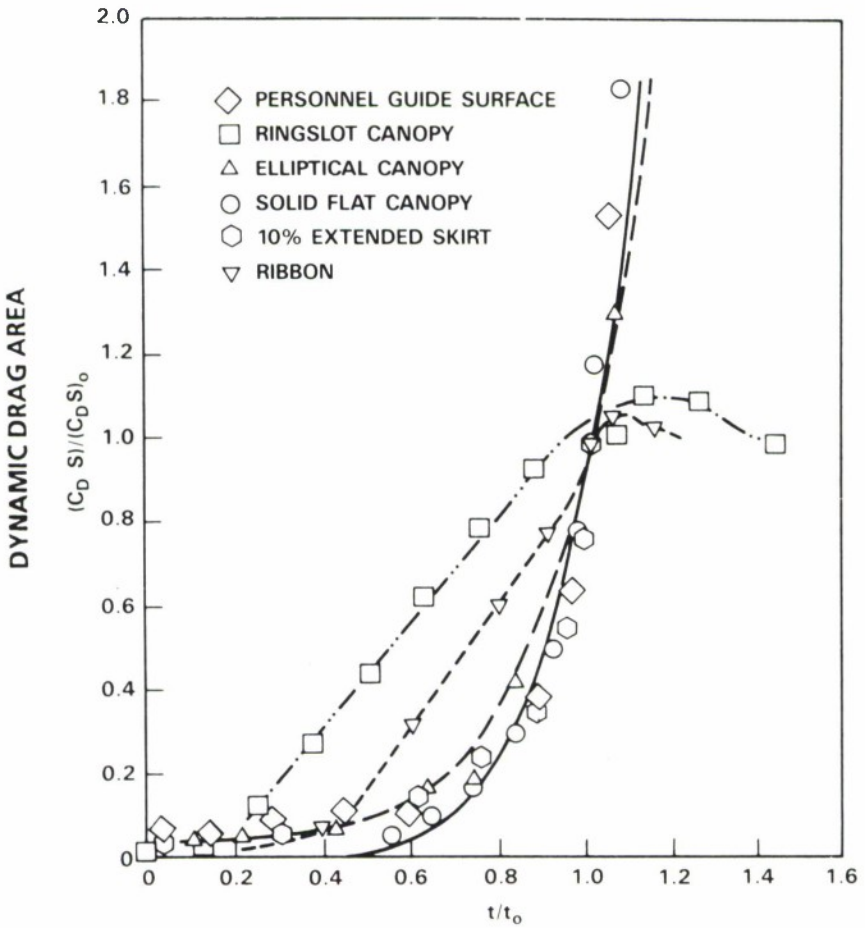

FIGURE 4. DYNAMIC DRAG AREA RATIO VERSUS TIME RATIO

Reference 3 adapts the drag area ratio to a wider range of applications by not assigning a particular value to the exponent. The form was introduced where

$$\frac{C_DS}{C_DS_O} = \left(\frac{t}{t_O}\right)^j \qquad ; \eta = \tau = 0 \tag{5}$$

j = 1 is indicative of geometrically porous parachutes and j = 6 represents the solid cloth family of parachutes.

The second step in the solution of Equation (1) is to develop an expression for the canopy rate of airflow. Parachute canopy airflow is discussed in another section of this report. The rate of airflow, P, through various canopy surface configurations can be expressed by the formula:

$$P = k(\Delta P)^n \qquad \Delta P = C_p q \tag{6}$$

then:

$$\Delta P = C_p \tfrac{1}{2} \rho V^2 \tag{6a}$$

$$P = k\left(\frac{C_p \rho V^2}{2}\right)^n$$

A basic mass flow equation for the solution of the inflation time and distance is obtained by substituting Equations (2), (3), (5), and (6a) into Equation (1).

$$\rho \frac{dV}{dt} = \rho V A_{MO} \left(\frac{t}{t_o}\right)^j - \rho\, A_{SO}\, k \left(\frac{C_p \rho}{2}\right)^n V^{2n} \left(\frac{t}{t_o}\right)^j \tag{7}$$

Measured values of n indicate a data range from 0.555 through 0.771. A convenient solution to the reference time equation for solid cloth parachutes evolves when n is assigned a value of 1/2, and j = 6.

$$\int_o^{V_o} dV = A_{MO} \int_o^{t_o} V \left(\frac{t}{t_o}\right)^6 dt - A_{SO}\, k \left(\frac{C_p \rho}{2}\right)^{1/2} \int_o^{t_o} V \left(\frac{t}{t_o}\right)^6 dt \tag{8}$$

The third step in the solution of Equation (1) is to determine the volume of air to be collected during inflation. The volume of air, V_o, associated with the steady state fully inflated parachute, is determined using the methods of Section VIII of Appendix A. By definition t_o is the particular instant during the inflation process when the transient parachute drag area is equal to the steady state drag area for the first time. The time required to collect the V_o volume of air is a function of the parachute type and geometry, canopy airflow properties, operational altitude, and trajectory velocity. The trajectory velocity variation during inflation is influenced by the system weight, parachute drag area, operational altitude, and trajectory angle at the line stretch velocity, V_S. Reference 4 applied Equation (8) to a vertical, toward the earth trajectory. Reference 5 applied Equation (8) to a general trajectory. Both of these references supply computer programs which use numerical integration to calculate the inflation reference time, t_o, and the opening shock force-deployment time profile. Reference 3 limited the trajectory to a horizontal direction. This approach develops an analysis that does not require the use of a computer. Solutions are readily obtained with a desk calculator for convenience. The horizontal force analysis derives closed form equations for the inflation velocity profile, shock factors and time of occurrence of the maximum force. The force analysis of Appendix A yields the velocity equation.

$$V = \frac{V_S}{1 + \frac{1}{7M}\left(\frac{t}{t_o}\right)^7} \qquad ; \eta = \tau = o \tag{9}$$

With the insertion of Equation (9) into Equation (7) for j = 6 yields.

$$\int_0^{V_O} dV = A_{MO} V_S \int_0^{t_O} \frac{\left(\frac{t}{t_O}\right)^6}{1 + \frac{1}{7M}\left(\frac{t}{t_O}\right)^7} dt - A_{SO} k \left(\frac{C_p \rho}{2}\right)^n \int_0^{t_O} \left(\frac{t}{t_O}\right)^6 \left[\frac{V_S}{1 + \frac{1}{7M}\left(\frac{t}{t_O}\right)^7}\right]^{2n} dt \quad (10)$$

The development of Equation (10) from Equation (1) has expressed the transient canopy volumes as a function of inflation reference time. This avoids the need to model or calculate specific intermediate geometric shapes. The only geometric shape that must be defined is the steady-state volume, V_O, and this is available. Equation (10), for a general value of n, requires a computer solution. Page 13 of Reference 4 defines important calculation considerations to be used in the solution.

A convenient solution to the reference time equation evolves when n is assigned a value of 1/2. Integrating Equation (10) and using :

$$V_S t_O M = \frac{2W}{\rho g C_D S_O}$$

$$t_O = \frac{14W}{V_S \rho g C_D S_O} \left[e^{\frac{g\rho V_O}{2W}\left[\frac{C_D S_O}{A_{MO} - A_{SO} k \left(\frac{C_p \rho}{2}\right)^{1/2}}\right]} \right]^{-1} \quad (11)$$

Multiplying both sides of Equation (11) by V_S demonstrates that $V_S t_o$ = A constant which is a function of altitude

$$V_S t_O = \frac{14W}{\rho g C_D S_O} \left[e^{\frac{g\rho V_O}{2W}\left[\frac{C_D S_O}{A_{MO} - A_{SO} k \left(\frac{C_p \rho}{2}\right)^{1/2}}\right]} \right]^{-1} \quad (12)$$

Equation (12) verifies axiom 1.

As a demonstration of Equation (11) the 35-foot D_0 diameter, 30-gore solid cloth cloth parachute of Example 1 of Reference 4 is to be applied. Deployment conditions are:

a. System weight = 200 lb.

b. Density altitude = 3,000 ft.

c. Air density = 0.0021753 slugs/ft^3.

d. Line stretch velocity = 340 fps

e. Drag coefficient = 0.75

f. Initial drag area, $\bar{\tau}$ = 0.

g. Trajectory angle, $\bar{\gamma} = 0^o$

h. Parachute surface area $S_o = 962.1\ ft^2$

i. Parachute drag area $C_D S_O = 721.6\ ft^2$

j. From Table 2, Page A-15 of Appendix A, the following inflated shape data were obtained for a 30-gore solid cloth flat circular parachute. See Figure 24 of Appendix A for shape nomenclature.

$$t_O = \frac{14 \times 200}{0.0021753 \times 32.2 \times 340 \times 721.58}\left[e^{K1} - 1\right]$$

k. Steady-state inflated canopy radius, $\bar{a} = 11.69$ ft

l. Steady-state mouth area, $A_{MO} = 399.53\ ft^2$

m. Steady-state canopy volume of air to be collected, V_O geometric = $4690.83\ ft^3$

The MIL-C-7020, type III canopy cloth airflow constant is k = 1.46 and the average pressure coefficient is taken to be Cp = 1.7 then:

$$K1 = \frac{32.2 \times 0.0021753 \times 4690.83}{2 \times 200}\left[\frac{721.58}{399.53 - 962.1\ (1.46)\left(\frac{0.0021753 \times 1.7}{2}\right)^{1/2}}\right] \quad (11)$$

$t_o = 0.773$ sec.

Knacke, Reference 7, presents the inflation time as

$$t_f = \frac{nD_o}{V_S} \quad (13)$$

where n = 8 for solid cloth parachutes

$$t_f = \frac{8 \times 35}{340}$$

$t_f = 0.824$ sec.

While Equation (13) is more convenient than (11) to use, Equation (11) gives the effects of altitude, mass, and cloth rate of airflow; both values are estimates of the inflation time. Equation (11) was theoretically derived. Equation (13) was empirically developed by other experimenters from numerous field test data. The parachute system of Example 1 deployed at an altitude of 1000 feet yields values of $t_o = 0.839$ second and $t_f = 0.824$ second. The closeness of the theoretical to and the empirical t_f values indicates that the application of the criterion listed below is a reasonable approach to the inflation time calculation.

a. Average pressure coefficient

b. Cloth permeability

c. The trajectory velocity is taken as the canopy inflow velocity.

d. The ratio of the instantaneous mouth area, A_M, to the steady-state mouth area, A_{MO}, is equal to the instantaneous drag-area ratio.

e. The ratio of the instantaneous pressurized canopy area, S, to the canopy surface area, S_o, is equal to the instantaneous drag-area ratio.

f. The volume of air to be collected during the inflation process is represented by V_O.

EFFECT OF DESIGN REQUIREMENTS ON PERFORMANCE

At the beginning of a parachute recovery system design, basic design requirements are laid down that determine the aerodynamic and geometric size of the decelerator. These requirements, together with decisions on the type of parachute to be applied, and canopy rate of airflow influence the operational performance of the design. Usually the basic requirements include the desired rate of descent, V_e, the altitude at which it is to be achieved, ρ, and the payload weight, W.

Once these decisions are firm the system W/C_DS_O has been established. At the equilibrium velocity the parachute drag force is equal to the system weight.

$$W = 1/2\rho V_e^2 \; C_D \; S_o$$

$$\frac{W}{C_D S_o} = 1/2\rho V_e^2 \qquad (14)$$

The particular system weight to be recovered defines the parachute aerodynamic size (C_DS_O). The geometric size (D_O) and inflated shape and volume are a result of the type of parachute and canopy rate of airflow selected.

$$C_D S_o = \frac{2W}{\rho V_e^2} \qquad (15)$$

The inflation distance is dependent on the parachute geometry, cloth airflow properties, W/C_DS_O, and altitude.

$$V_{St_O} = \frac{14W}{\rho g C_D S_O}\left[e^{\frac{g\rho V_O}{2W}\left[\frac{C_D S_O}{A_{MO}-A_{SO}\,k\left(\frac{C_p\rho}{2}\right)^{1/2}}\right]}\right]^{-1} \qquad (12)$$

When the parachute type, canopy cloth, and suspension line length have been selected, the only variable undefined is the operational altitude. The inflation distance does not depend on the velocity at suspension line stretch, but the inflation reference time does. Rather, the inflation distance has been preordained by the system requirements, and initial design decisions. For a given recovery system and operational deployment altitude the inflation distance is a constant.

Now let's examine axiom 2. Table 1 of Reference 3 summarizes the parachute performance formulas for several values of j. Parachute performance for horizontal deployment depends on the type of parachute, j, initial drag area, C_DS_i, and the Ballistic Mass Ratio (BMR), M, which is not a function of the parachute velocity at suspension line stretch, but does depend on the inflation distance and operational altitude.

$$M = \frac{2W}{\rho g V_s t_o C_D S_o} \tag{16}$$

The time of the occurrence of the maximum shock factor during the finite mass process, and the maximum shock factor are defined by the BMR. For solid cloth parachutes; j=6, let $\tau = 0$.

$$\left(\frac{t}{t_o}\right)@\ x_{i\ max} = \left(\frac{21M}{4}\right)^{1/7} \tag{17}$$

$$x_{i\ max} = \frac{16}{49}\left(\frac{21M}{4}\right)^{6/7} \tag{18}$$

The BMR is the scale parameter which determines what percentage of the steady state drag force, F_S, is to be realized as opening shock force.

$$F_S = 1/2\rho V_S^2 C_D S_o \tag{19}$$

Example 1: A Test of axiom 2

A given finite mass parachute system is to be tested at several operational velocities at a given altitude. Examine the opening shock performance and graph the variation of the maximum shock force, F_{max}, versus inflation reference time, t_o. What conclusions are evident?

Solution: The system is tested at an initial line stretch velocity, V_S. The inflation distance $V_S t_o$ from Equation (12), is independent of velocity and is determined by the parachute geometry, altitude, and cloth airflow. The inflation distance is used to determine the BMR of Equation (16). The time of occurrence during the inflation process, Equation (17), and the maximum shock factor, (Equation (18)), are determined by the BMR. The line stretch velocity only affects operational performance in the steady state drag calculation, (Equation (19)). The maximum shock force, F_{max} is given by:

$$F_{max} = x_{i_{max}} F_S \tag{20}$$

For a given altitude and line stretch velocity V_S the inflation distance is determined by Equation (12) and F_{max} by Equation (20). If the test velocity is doubled the inflation distance is unchanged. This means that the BMR, time of occurrence, and maximum shock factor remain unchanged. However, the steady-state drag has increased by a factor of four. The maximum shock force increases because the constant shock factor of the system is claiming the same percentage of a much higher force. From Equation (12) the doubling of the velocity reduces the inflation reference time by 1/2. If the test velocity is reduced by 1/2 the inflation reference time increases by a factor of two and the maximum shock force is reduced by a factor of 1/4 due to the reduction of the steady-state drag force.

These data are plotted in Figure 5. First examination of Figure 5 would seem to demonstrate that the maximum force is a strong function of inflation time. However, the maximum shock force varied because the steady state drag force varied due to changing V_S, not because the inflation reference time was altered.

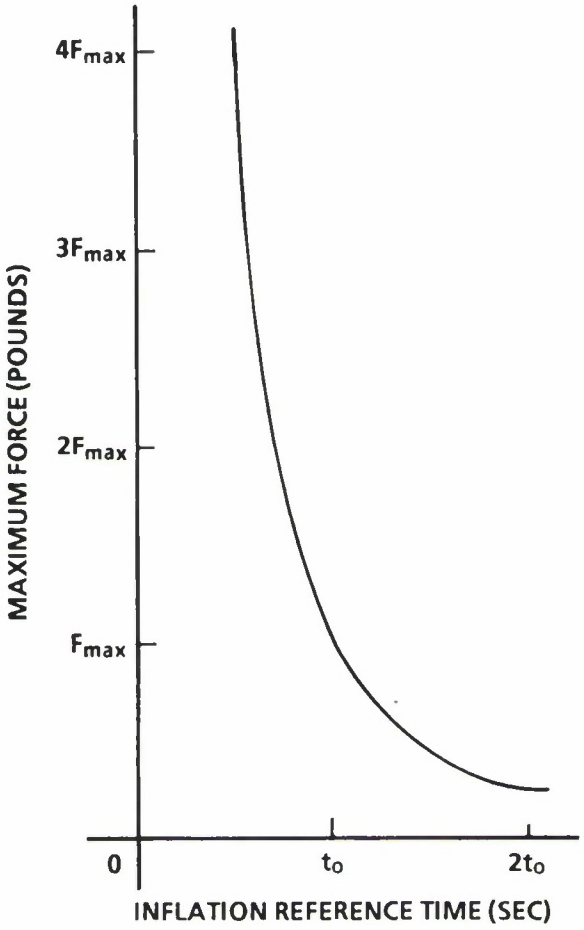

FIGURE 5. APPARENT VARIATION OF MAXIMUM PARACHUTE OPENING SHOCK FORCE WITH INFLATION REFERENCE TIME

The conclusion to be drawn from Figure 5 is that axiom 2 appears to be true, but is not. The inflation distance is more important to the inflation process than the inflation reference time.

Since the inflation distance is constant V_s can be expressed as:

$$V_s = \frac{\text{Constant}}{t_o}$$

in which case Equation (20) can be expressed as

$$F_{max} = x_{i_{max}} \frac{\rho C_D S_o}{2} \left(\frac{\text{Constant}}{t_o}\right)^2 \qquad (20a)$$

This approach does show the inverse parabolic variation of opening shock force with inflation reference time, but t_o is a dependent variable of V_s which is not a reversible process. So, even though Equation (20a) is mathematically valid it does not express the problem in a usable form. It is physically possible to specify a line

stretch velocity. The specified line stretch velocity results in a specific inflation reference time. It is NOT physically possible to specify only an inflation reference time and have this result in a specific line stretch velocity.

DISCUSSION OF THE VARIABLES OF THE INFLATION REFERENCE TIME AND DISTANCE EQUATIONS

$$V_{St_O} = \frac{14W}{\rho g C_D S_O}\left[e^{\frac{g\rho V_O}{2W}\left[\frac{C_D S_O}{A_{MO}-A_{SO}\,k\left(\frac{C_p\rho}{2}\right)^{1/2}}\right]}\right]^{-1} \qquad (12)$$

The inflation distance (V_{St_o}) appears to be a velocity-time effect. Equation (12) indicates that the inflation distance actually depends on system mass ratios, area ratios and canopy airflow properties. The several terms of Equation (12) each have a physical significance on parachute performance. The following paragraphs identify and explain the meaning of each term.

Weight-to-drag area ratio, W/C_DS_O

The identical parachute used in finite mass, intermediate mass, or infinite mass systems experiences a variation in inflation time due to its mode of use. Low weight-to-drag area ratios in the range of 0.3 suggest low rate of descent finite mass deployments as in the recovery of personnel. High rate of descent infinite mass applications, as in ordnance usage, may have weight-to-drag area ratios in excess of thirty four. Equations (11) and (12) are applicable to all modes of operation. At the time t_o all inflations have collected the same volume of air. Finite mass inflations experience a significant velocity reduction during the inflation process which limits the rate of airflow into the canopy and extends the inflation time. Infinite mass deployments, on the other hand, can be nearly constant velocity which maintains a higher rate of mass flow into the canopy and decreases the inflation time. Actual constant velocity infinite mass operation produces the minimum inflation time. The inflation reference times, for the parachute of Example 1, are plotted in Figure 6 as a function of weight-to-drag-area ratio for Equation (11). The finite mass and infinite mass limiting Ballistic Mass Ratios for solid cloth parachutes are referenced on the graph. An arbitrary Ballistic Mass Ratio value of 10 was selected as the boundary between intermediate mass and infinite mass operation for solid cloth parachutes. Figure 9 of Appendix A shows a minimal velocity reduction at $t/t_o = 1$ for a BMR of 10 when compared to true infinite mass.

The trends of Figure 6 show that the principal variation of the inflation reference time occurs in the finite mass mode of operation. By the transition from finite mass to low intermediate mass, a near minimum inflation reference time is reached. This quickly converges to an essentially constant value for the high end of the intermediate mass and infinite mass regimes. Similar trends for other types of parachutes are a reasonable extension of the premise since it is based on variable rates of flow filling a constant volume.

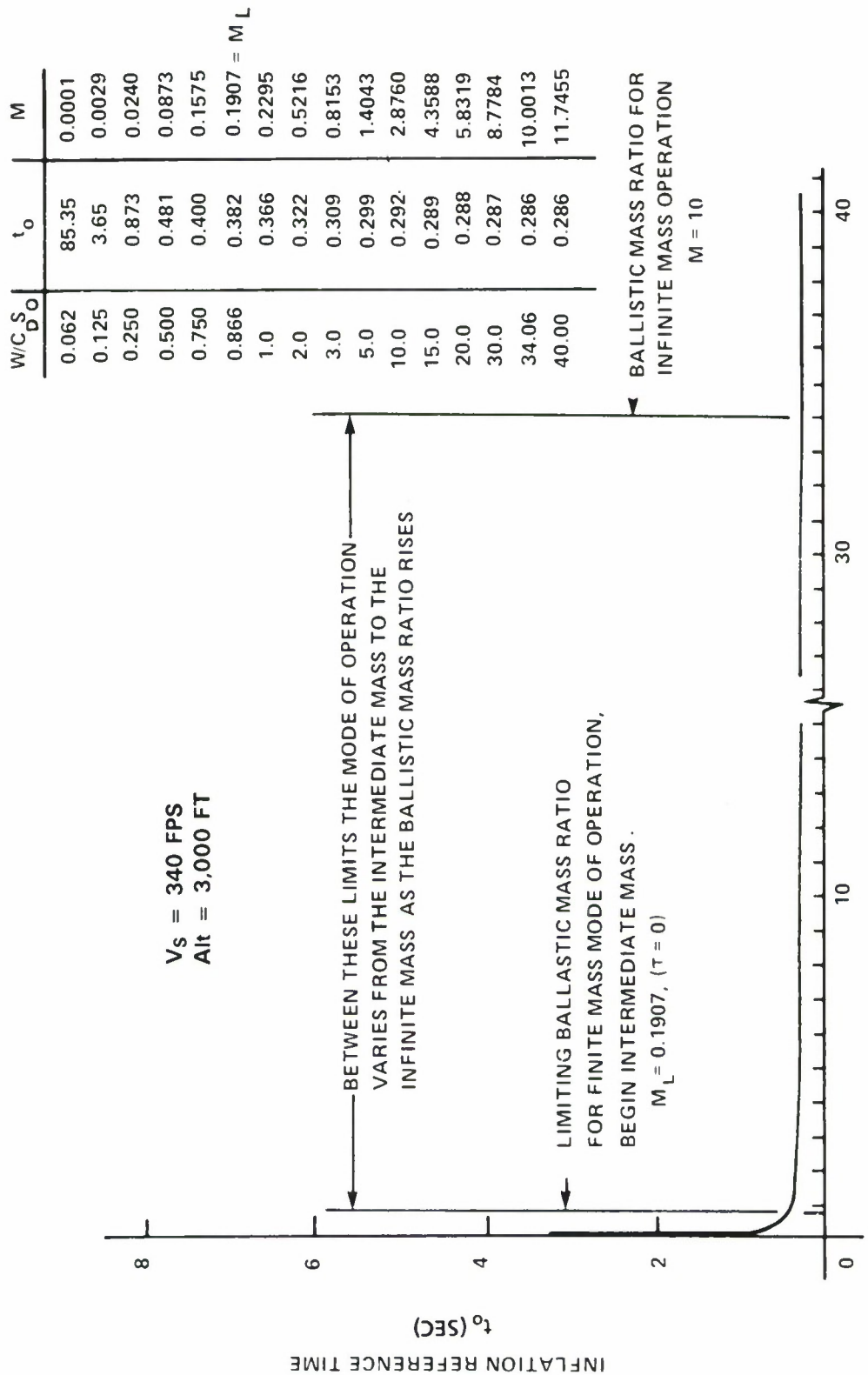

W/C_DS_O	t_o	M
0.062	85.35	0.0001
0.125	3.65	0.0029
0.250	0.873	0.0240
0.500	0.481	0.0873
0.750	0.400	0.1575
0.866	0.382	0.1907 = M_L
1.0	0.366	0.2295
2.0	0.322	0.5216
3.0	0.309	0.8153
5.0	0.299	1.4043
10.0	0.292	2.8760
15.0	0.289	4.3588
20.0	0.288	5.8319
30.0	0.287	8.7784
34.06	0.286	10.0013
40.00	0.286	11.7455

FIGURE 6. VARIATION OF THE INFLATION REFERENCE TIME AS A FUNCTION OF SYSTEM WEIGHT FOR THE FLAT CIRCULAR SOLID CLOTH PARACHUTE OF EXAMPLE ONE

Coefficient $14W/(\rho g C_D S_o)$

This coefficient is the ratio of the system mass (W/g) to an atmospheric mass ($\rho C_D S_o$) per foot of length of the Ballistic Mass Ratio atmosphere cylinder of Figure 8 of Appendix A.

Exponent coefficient $g\rho V_o/2W$

This dimensionless coefficient in the exponent is the ratio of the mass of atmosphere associated with the steady-state inflated canopy (ρV_o) to the system mass (W/g).

Inflation Time and Distance Exponent Dimensionless Area Ratio Term

The dimensionless area ratio expression is the ratio of the parachute aerodynamic size ($C_D S_o$) to the effective mouth area expressed in the denominator. As the rate of flow through the canopy varies with k, ρ,n, or pressure coefficient, the inflation characteristics are modified.

when:
$$O = A_{Mo} - A_{so} k \left(\frac{C_p \rho}{2} \right)^{1/2} \tag{21}$$

A critical condition exists and the parachute fails to fully inflate. As the effective mouth area approaches zero, t_o increases exponentially. It is possible for the inflation time to be extended to the point that the parachute system is not practical even though the effective mouth area is not zero. If the critical parachute system is deployed at a higher altitude the air density reduction causes the effective mouth area to become positive and the canopy inflates. Imporous canopies ($k = 0$) always inflate. These phenomena agree with field test observations.

As a demonstration of the cloth rate of airflow effects in Equation (11), replacement of the canopy cloth of Example 1 with a high rate of airflow, three momme silk cloth ($k = 7.43$), yields an inflation reference time of $t_o = 99.76$ sec. under the Example 1 operational conditions. This time exceeds the time of fall from 3,000 feet and the system would appear to an observer as a partial inflation. The same system deployed horizontally at 20,000 feet, at constant dynamic pressure, has an inflation reference time of $t_o = 1.5$ sec.

The effective mouth area is a clue in the solution of the parachute critical velocity phenomenon. Another part of the problem is the effect of suspension line length and number of gores in the canopy. Consider the parachute as consisting of two main elements. A canopy which generates the aerodynamic force, and a number of suspension lines that transmit the force to the payload. The two elements are joined at the canopy skirt hem to complete the parachute assembly. The parachute inflation characteristics depend on the force distribution at the canopy skirt hem, see Figure 7. Due to the cone angle of the suspension lines there is a radial component of the suspension line force, F_{SL}, normal to the canopy centerline that tends to collapse

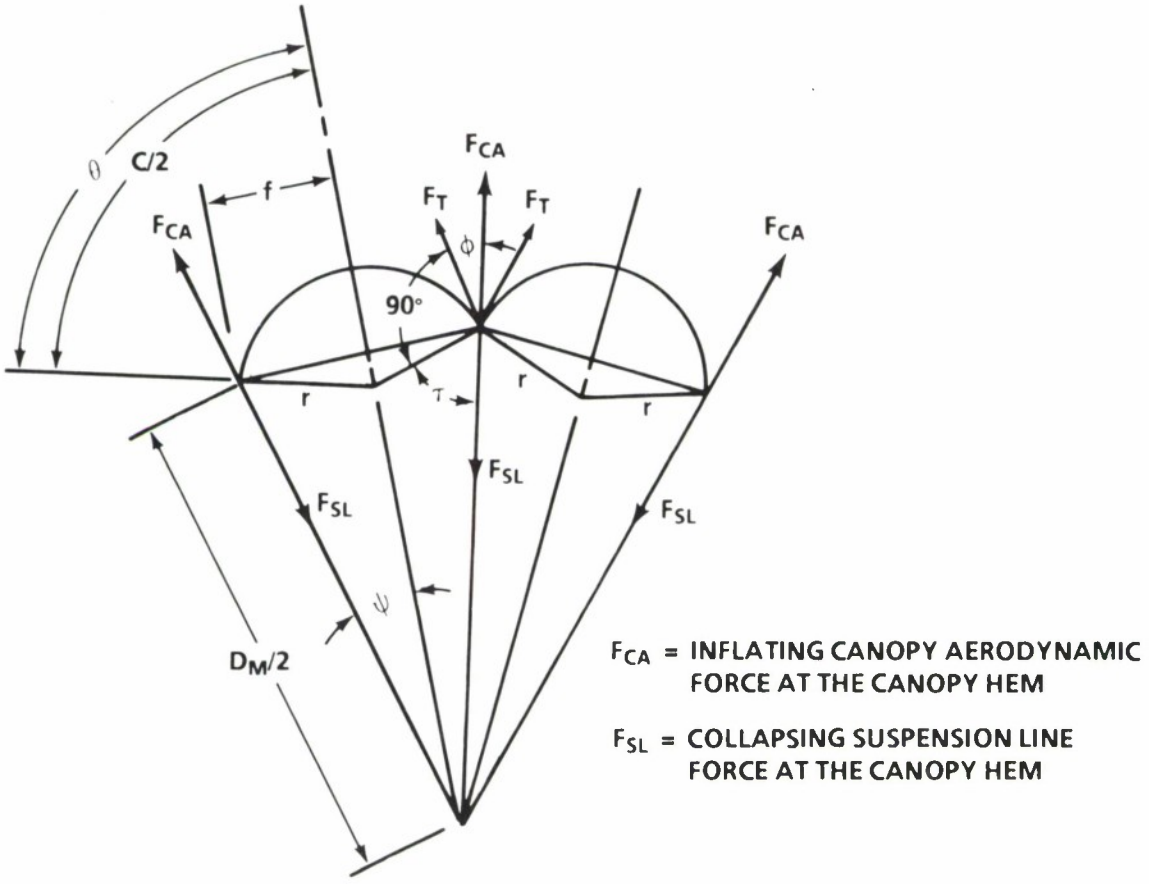

FIGURE 7. CANOPY SKIRT HEM GEOMETRY AND FORCE DISTRIBUTION OF FLAT PARACHUTES IN FULL STEADY-STATE INFLATION

the canopy. The radial component of the canopy aerodynamic force, F_{CA}, tends to inflate the canopy. At full or partial steady-state inflation, the outward radial component of the canopy inflating aerodynamic force is in balance with the suspension line collapsing normal force component. Partial inflations produce a pseudo hem where the inflated and uninflated canopy sections meet. During the inflation process the velocity head of the fluid entering the canopy is reduced, resulting in an increase in canopy internal pressure. As long as the fluid inflow exceeds the outflow, additional fluid volume is added to the canopy and the internal pressure wave advances. When the outflow is equal to the inflow, the velocity of the flowing fluid is not reduced and additional higher pressure fluid is not added to the volume. The internal pressure is sustained at the partially inflated level.

The suspension line length and the number of canopy gores contribute to the equilibrium diameter size of the partially inflated parachute. Lengthening the suspension lines improves inflation characteristics by reducing the radial force component tending to collapse the canopy. Shortening the suspension lines has the opposite effect. Increasing the number of gores in the canopy reduces the angle ϕ, Figure 7, between the tangent force in the cloth, F_T, in the main seam and the canopy mouth diameter. This angular reduction uses the canopy aerodynamic force more

efficiently and contributes to inflation. In the limit, angle ϕ approaches zero degree as the number of gores approaches infinity. There are three combined contributing factors to parachute critical velocity.

a. Canopy rate of airflow - Determines the ability of the canopy to entrap the volume of fluid, V_O, required for full inflation. See the cloth rate of airflow section for the effects of altitude, k, and n.

b. Length of the suspension lines.

c. Number of gores in the canopy.

The interrelationship of these three factors control the inflation characteristics of each design.

EFFECTS OF ALTITUDE ON THE INFLATION REFERENCE TIME AND DISTANCE

Numerous simplified filling time equations have been published in many reports and will not be repeated here. Generally there are two forms:

$$t_f = \frac{nD_0}{V_s^{0.9}} \tag{23}$$

$$t_f = \frac{nD_0}{V_s} \tag{24}$$

Figure 8 shows that when V_S is raised to the 0.9 power, the result is nearly the same as dividing V_S by 2. So Equation (23) can be simplified by multiplying n by 2 and setting the exponent of V_s to unity.

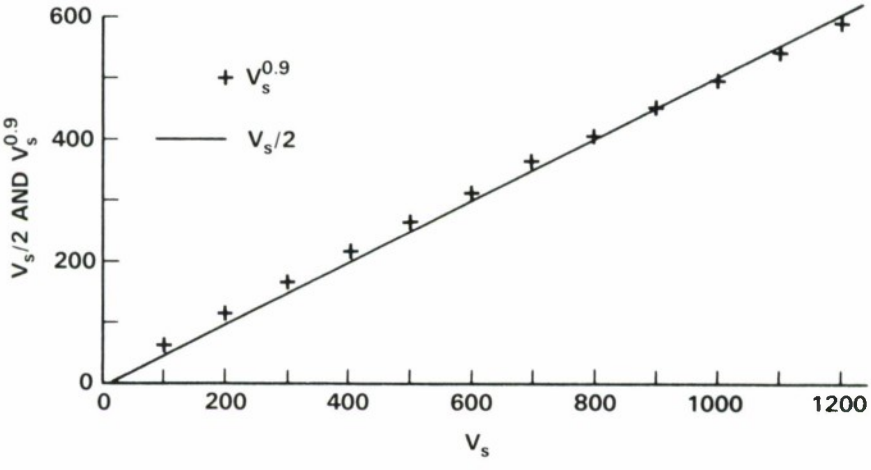

FIGURE 8. EFFECT OF THE FILLING TIME EQUATION EXPONENT 0.9 ON THE TRAJECTORY VELOCITY AT PARACHUTE SUSPENSION LINE STRETCH

The accepted values of n for Equation (24) are 8 for solid cloth parachutes and 14 for geometrically porous. Table 1 lists canopy fill factors for various types of parachutes.

TABLE 1. CANOPY FACTOR, n, FOR VARIOUS PARACHUTE TYPES

PARACHUTE TYPE	CANOPY FILL FACTOR, n		
	REEFED OPENING	DISREEF OPENING	UNREEFED OPENING
SOLID FLAT CIRCULAR	ID[1/]	ID	8
EXTENDED SKIRT, 10%	16-18	4-5	10
EXTENDED SKIRT, FULL	16-18	7	12
CROSS	ID	ID	11.7
RIBBON	10	6	14
RINGSLOT	ID	ID	14
RINGSAIL	7-8	2	7
RIBLESS GUIDE SURFACE	...	...	4-6

[1/] ID = INSUFFICIENT DATA AVAILABLE FOR MEANINGFUL EVALUATION

Reproduced from Reference 7

Figure 9 compares the inflation times calculated by Equations (11) and (24) for a 35-foot D_O, T-10 type canopy deployed at a sea level line stretch velocity of V_S = 211 fps with a system weight of 200 lbs. Figure 9 shows the time variation for altitudes up to 50,000 feet when testing at constant dynamic pressure.

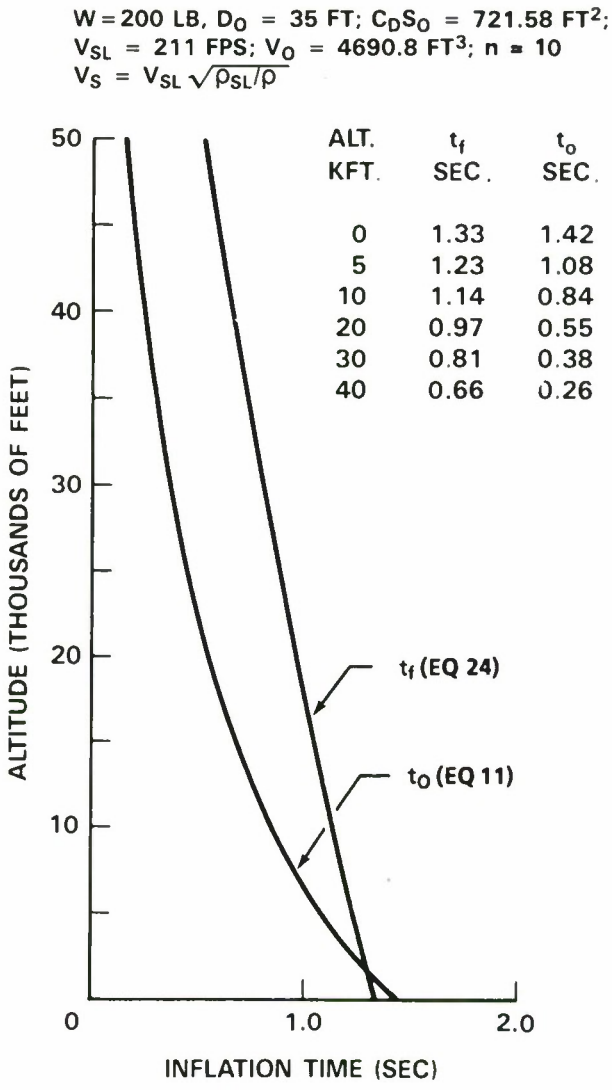

FIGURE 9. VARIATION OF INFLATION TIME FOR A T-10 TYPE PARACHUTE SYSTEM AS A FUNCTION OF EMPERICAL AND DERIVED METHODS OF CALCULATION FOR VARIOUS ALTITUDES

The inflation time of Equation (24) produces an apparent reduction in inflation time due to the increase in V_S to maintain a constant dynamic pressure.

The decrease in inflation reference time in Equation (11) is due to the decrease in air density. For constant dynamic pressure as altitude increases the test velocity must be varied.

Substituting for V_S into Equation (11) and simplifying

$$t_o = \frac{14W}{gC_D S_o V_{SL}\sqrt{\rho\rho_{SL}}} \left[e^{\frac{g\rho V_o}{2W}\left[\frac{C_D S_o}{A_{MO}-A_{SO}\,k\left(\frac{C_p\rho}{2}\right)^{1/2}}\right]} \right]^{-1} \qquad (11a)$$

At all altitudes the V_{SL} remains constant, and the primary variable is density. Other possible variations may be due to drag coefficient rise caused by a decrease in canopy cloth airflow properties and possible changes in geometry caused by the rise in drag coefficient. Otherwise, the reference time is only a function of system constants and altitude.

As actual values of the rate of fluid flow exponent n approach 1.0 the inflation reference time and distance are extended. Equation (7) was programmed in Reference 5 for values of n other than 0.5 and the effects of an arbitrary trajectory angle at deployment for j = 6. Figure 10 illustrates the effects of altitude, n, and trajectory deployment angle for a constant velocity at all altitudes, and Figure 11 illustrates the same variables for a constant dynamic pressure at all altitudes. Figure 12 presents the effects of n and altitude on the inflation reference time for constant velocity and constant dynamic pressure for horizontal deployment. At sea level the extension of the inflation reference time due to a realistic n = 0.632 is evident. Solid cloth parachutes inflate more rapidly at higher altitudes due to the decrease in air density. At constant trajectory velocity or constant dynamic pressure the effects of the particular value of n converge and the inflation time is essentially independent of n and k. Therefore, Equation (11) for high altitude horizontal trajectories is appropriate. The inflation distance versus altitude of Figure 13 for n = 0.500 is the same whether constant velocity or dynamic pressure profile is used. The realistic n = 0.632 of Figure 14 gives a slight variation in inflation distance.

APPLICATION OF CLOTH PERMEABILITY TO THE CALCULATION OF THE INFLATION TIME OF PARACHUTES

The mass outflow through the pressurized region of an inflating parachute at any instant is dependent upon the instantaneous canopy area which is subjected to airflow and the rate of airflow through that area. The variation of pressurized canopy surface area as a function of reference time ratio t/t_o, was earlier defined as being proportional to the instantaneous drag area ratio, leaving the rate-of-airflow problem to solve. The permeability parameter of cloth was a natural choice for determining the rate of airflow through the cloth as a function of pressure differential across the cloth. Heretofore, these data have been more of a qualitative, rather than quantitative, value. A method of analysis was developed wherein a generalized curve of the form $P = k(\Delta P)^n$ was fitted to the cloth permeability data for a number of different cloths and gives surprisingly good agreement over the pressure differential range of available data. The pressure differential was related to the trajectory velocity and altitude conditions to give a generalized expression which can

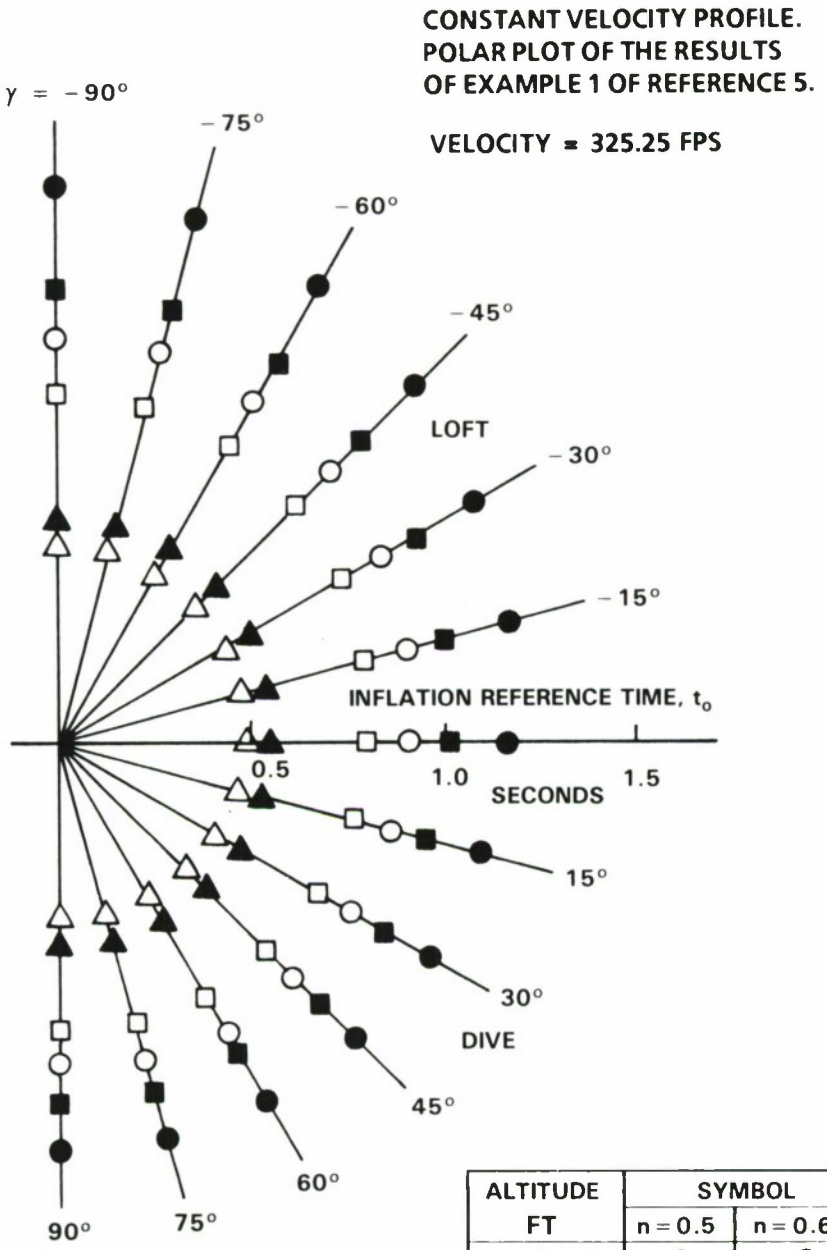

ALTITUDE	γ (DEG)	n = 0.500 t_o (SEC)	n = 0.662 t_o (SEC)
SEA LEVEL	−90	1.054	1.416
	−75	1.047	1.401
	−60	1.026	1.362
	−45	0.998	1.311
	−30	0.970	1.259
	−15	0.940	1.213
	0	0.913	1.171
	15	0.894	1.138
	30	0.874	1.108
	45	0.860	1.088
	60	0.849	1.074
	75	0.841	1.065
	90	0.839	1.062
3,000 FT	−90	0.904	1.171
	−75	0.900	1.163
	−60	0.894	1.142
	−45	0.876	1.111
	−30	0.854	1.079
	−15	0.833	1.046
	0	0.813	1.018
	15	0.794	0.992
	30	0.779	0.972
	45	0.767	0.955
	60	0.758	0.944
	75	0.753	0.938
	90	0.751	0.936
20,000 FT	−90	0.513	0.590
	−75	0.512	0.589
	−60	0.509	0.585
	−45	0.504	0.579
	−30	0.499	0.572
	−15	0.493	0.565
	0	0.486	0.559
	15	0.481	0.551
	30	0.476	0.545
	45	0.471	0.539
	60	0.469	0.537
	75	0.467	0.534
	90	0.466	0.534

FIGURE 10. EFFECTS OF TRAJECTORY LAUNCH ANGLE, ALTITUDE, AND CLOTH RATE OF AIRFLOW ON THE PARACHUTE INFLATION REFERENCE TIME AT CONSTANT VELOCITY, EXAMPLE 1 OF REFERENCE

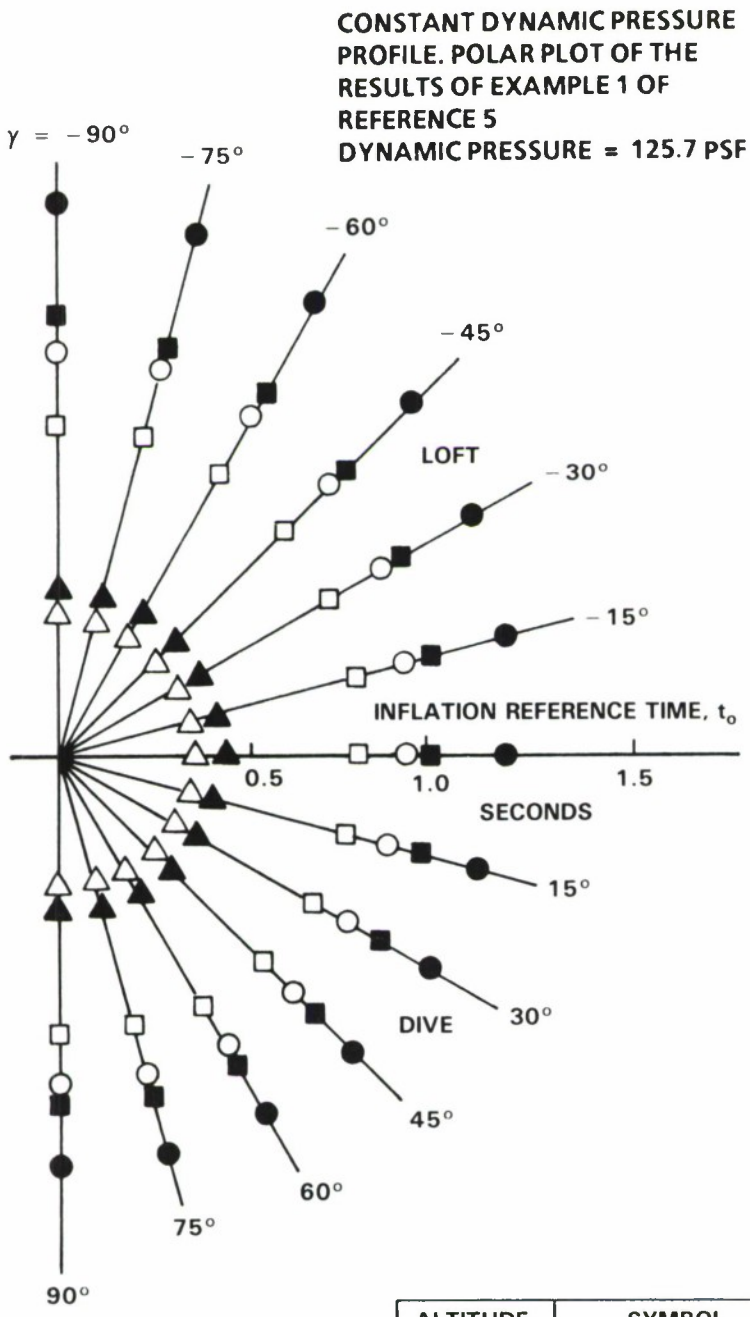

ALTITUDE FT	SYMBOL n = 0.5	SYMBOL n = 0.632
0	○	●
3,000	□	■
20,000	△	▲

ALTITUDE	γ (DEG)	n = 0.500 t_o (SEC)	n = 0.662 t_o (SEC)
SEA LEVEL	−90	1.054	1.418
	−75	1.048	1.400
	−60	1.027	1.363
	−45	0.999	1.312
	−30	0.968	1.260
	−15	0.941	1.214
	0	0.913	1.172
	15	0.894	1.138
	30	0.874	1.109
	45	0.860	1.089
	60	0.850	1.074
	75	0.842	1.066
	90	0.840	1.063
3,000 FT	−90	0.862	1.115
	−75	0.859	1.109
	−60	0.849	1.090
	−45	0.834	1.065
	−30	0.814	1.036
	−15	0.795	1.008
	0	0.778	0.982
	15	0.762	0.958
	30	0.749	0.941
	45	0.738	0.925
	60	0.730	0.916
	75	0.725	0.909
	90	0.724	0.908
20,000 FT	−90	0.366	0.433
	−75	0.365	0.433
	−60	0.364	0.432
	−45	0.362	0.429
	−30	0.361	0.428
	−15	0.358	0.425
	0	0.357	0.422
	15	0.354	0.419
	30	0.352	0.416
	45	0.350	0.414
	60	0.349	0.412
	75	0.348	0.411
	90	0.348	0.411

FIGURE 11. EFFECTS OF TRAJECTORY LAUNCH ANGLE, ALTITUDE, AND CLOTH RATE OF AIRFLOW ON THE PARACHUTE INFLATION REFERENCE TIME AT CONSTANT DYNAMIC PRESSURE, EXAMPLE 1 OF REFERENCE 5

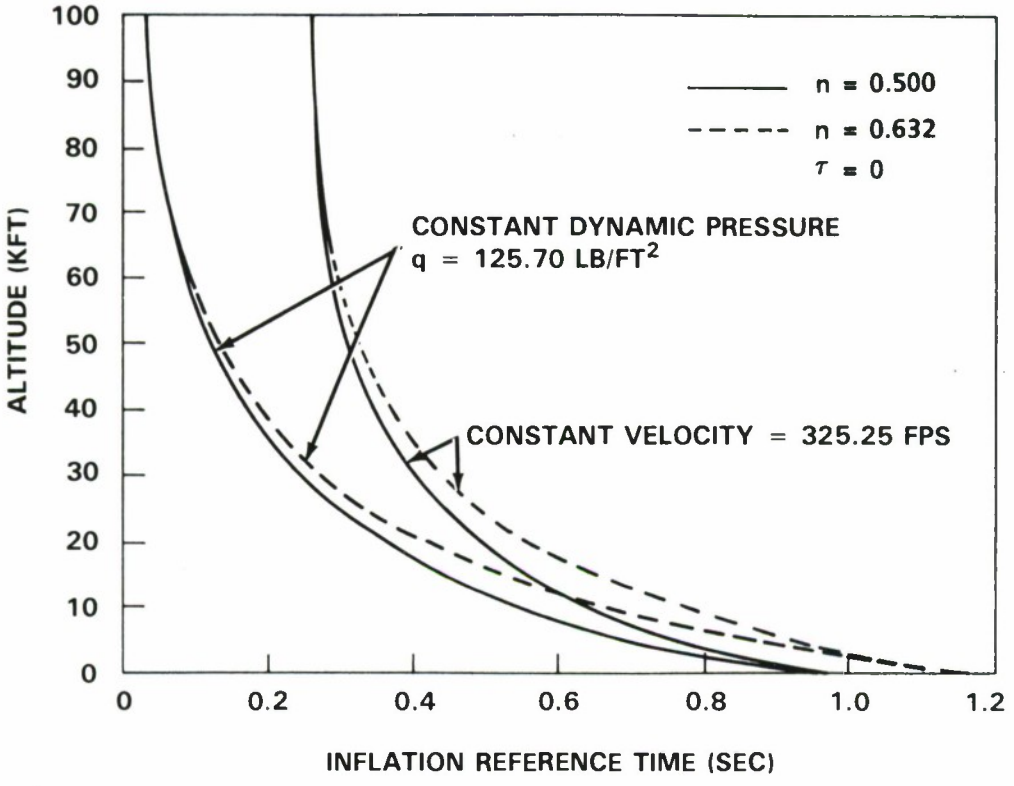

FIGURE 12. EFFECT OF ALTITUDE ON THE INFLATION REFERENCE TIME "T_O"

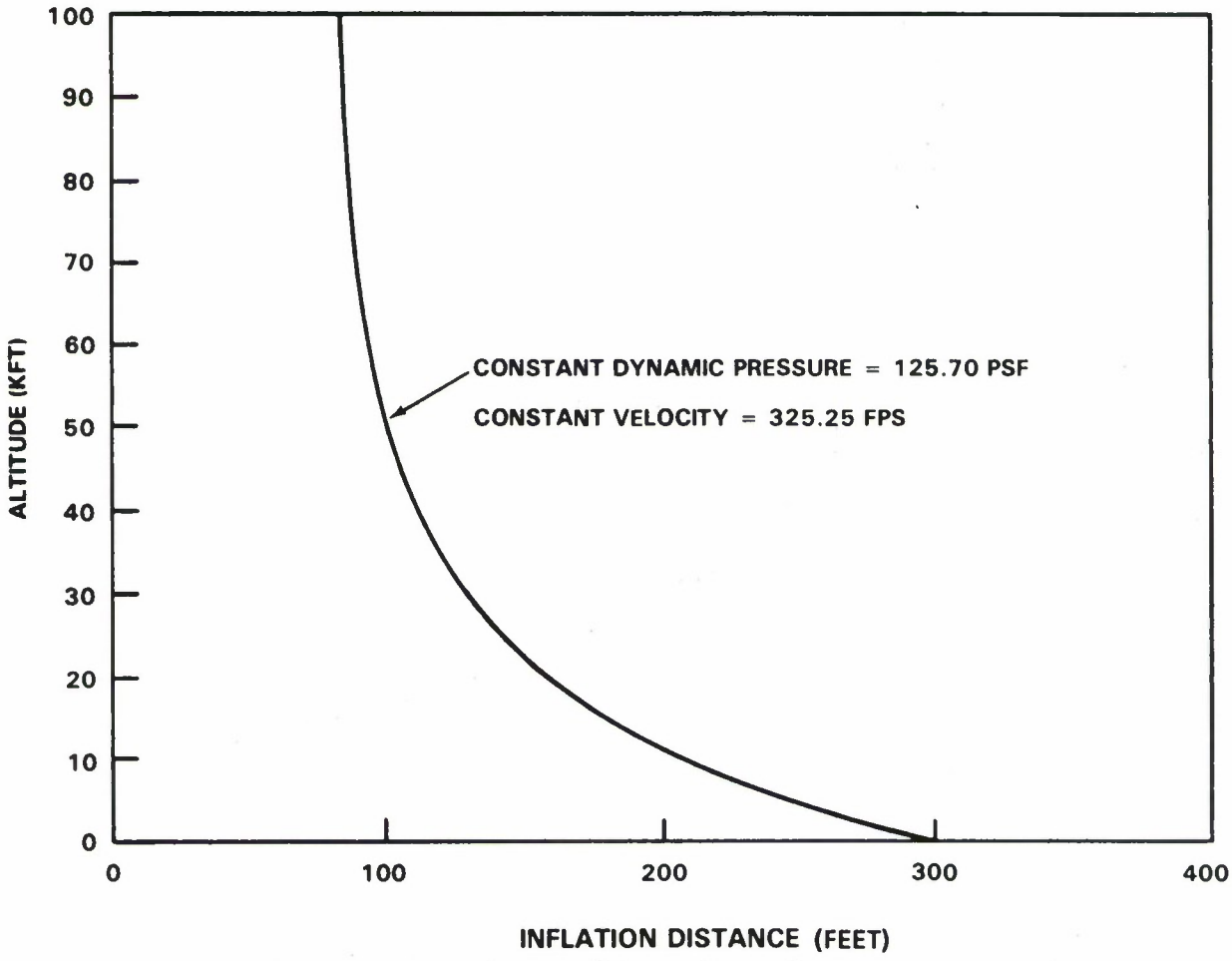

FIGURE 13. EFFECT OF ALTITUDE ON THE INFLATION DISTANCE
$n = 0.500, \gamma = 0°, \bar{\tau} = 0$

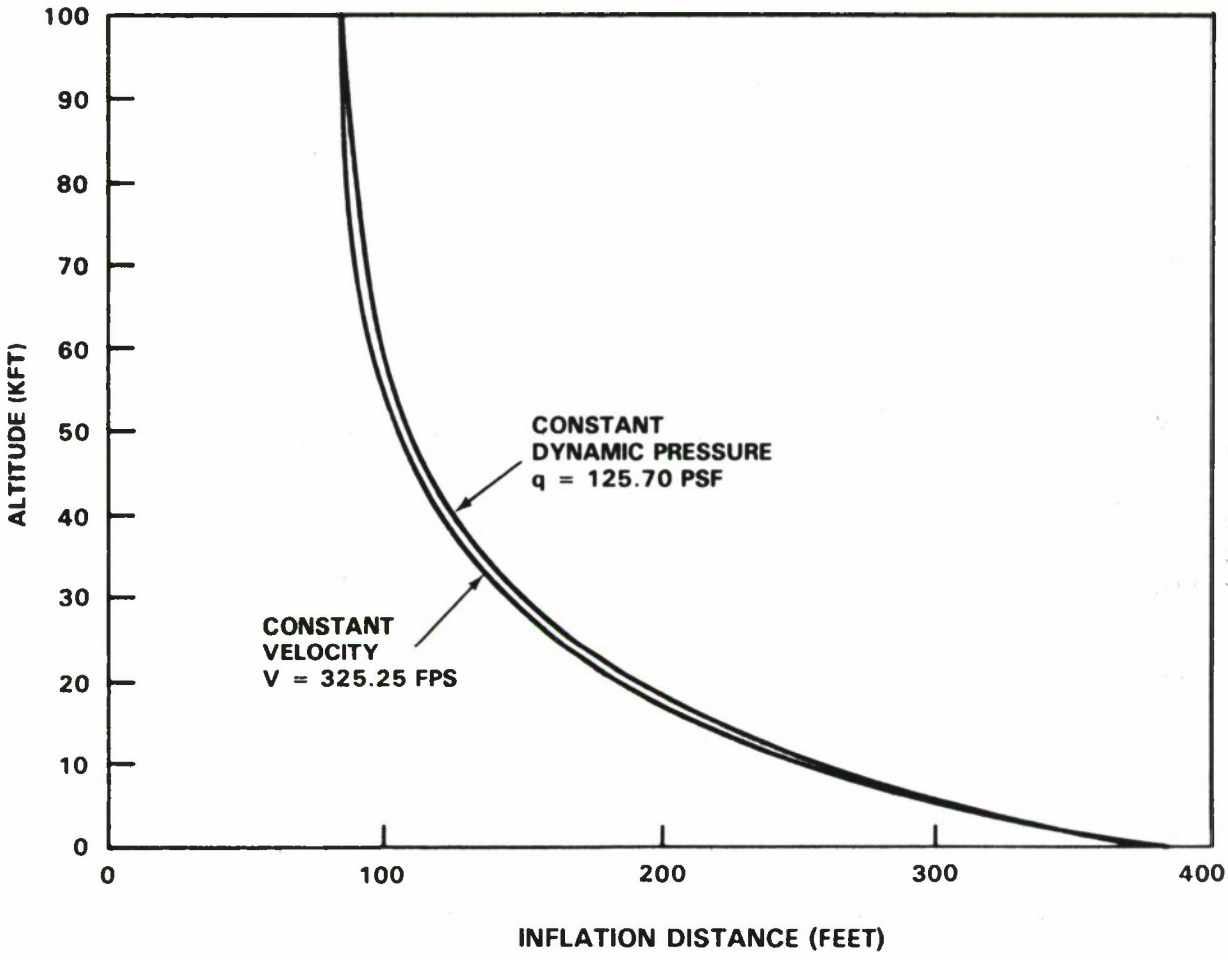

FIGURE 14. EFFECT OF ALTITUDE ON THE INFLATION DISTANCE
N = 0.632, $\gamma = 0^{\circ}$, $\tau = 0$

be used in the finite, intermediate, and infinite Ballistic Mass Ratio ranges. This approach varies the rate of airflow for the particular trajectory conditions at each instant during inflation.

Measured and calculated permeability pressure data for several standard cloths are illustrated in Figure 15. This method has been applied to various types of cloth between the extremes of a highly permeable 3-momme silk to a relatively impervious parachute pack container cloth with reasonably good results, see Figure 16.

The canopy average pressure coefficient, C_p, is defined as the ratio of the pressure differential across the cloth to the dynamic pressure of the free stream.

$$C_p = \frac{\Delta P}{q} = \frac{P(\text{internal}) - P(\text{external})}{1/2\ \rho V^2} \tag{25}$$

where V is the instantaneous trajectory velocity.

The permeability expression, $P = k(\Delta P)^n$ becomes

$$P = k\left(C_p \frac{\rho V^2}{2}\right)^n \tag{6a}$$

The inflation time of solid cloth parachutes decreases as the operational altitude increases. This effect can be explained by considering the ratio of the mass outflow through a unit cloth area to the mass inflow through a unit mouth area.

$$M' = \text{mass flow ratio} = \frac{\text{mass outflow}}{\text{mass inflow}}$$

where

$$\text{mass outflow} = P\rho \frac{\text{slugs}}{\text{ft}^2\,\text{sec}} (\text{per ft}^2 \text{ cloth area})$$

and

$$\text{mass inflow} = V\rho \frac{\text{slugs}}{\text{ft}^2\,\text{sec}} (\text{per ft}^2 \text{ inflow area})$$

Therefore, the mass flow ratio becomes

$$M' = \frac{\rho P}{\rho V} = \frac{P}{V}$$

$$M' = k\left(\frac{C_p \rho}{2}\right)^n V^{(2n-1)} \tag{26}$$

Effective porosity C, is defined as the ratio of the velocity through the cloth, u, to a fictitious theoretical velocity, v, which will produce the particular $\Delta P = \rho v^2/2$.

$$\text{effective porosity, } C = u/v \tag{27}$$

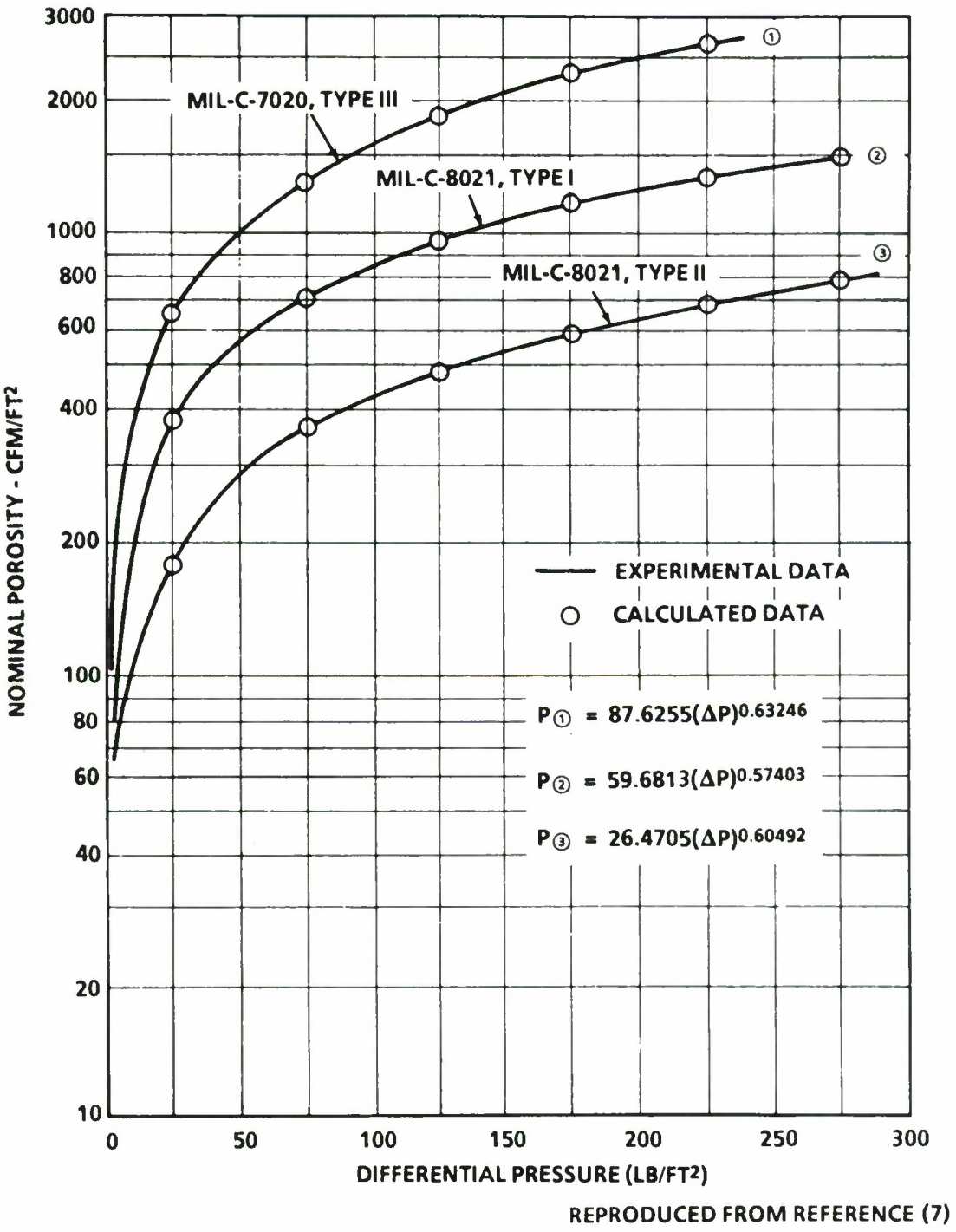

FIGURE 15. NOMINAL POROSITY OF PARACHUTE MATERIAL VERSUS DIFFERENTIAL PRESSURE

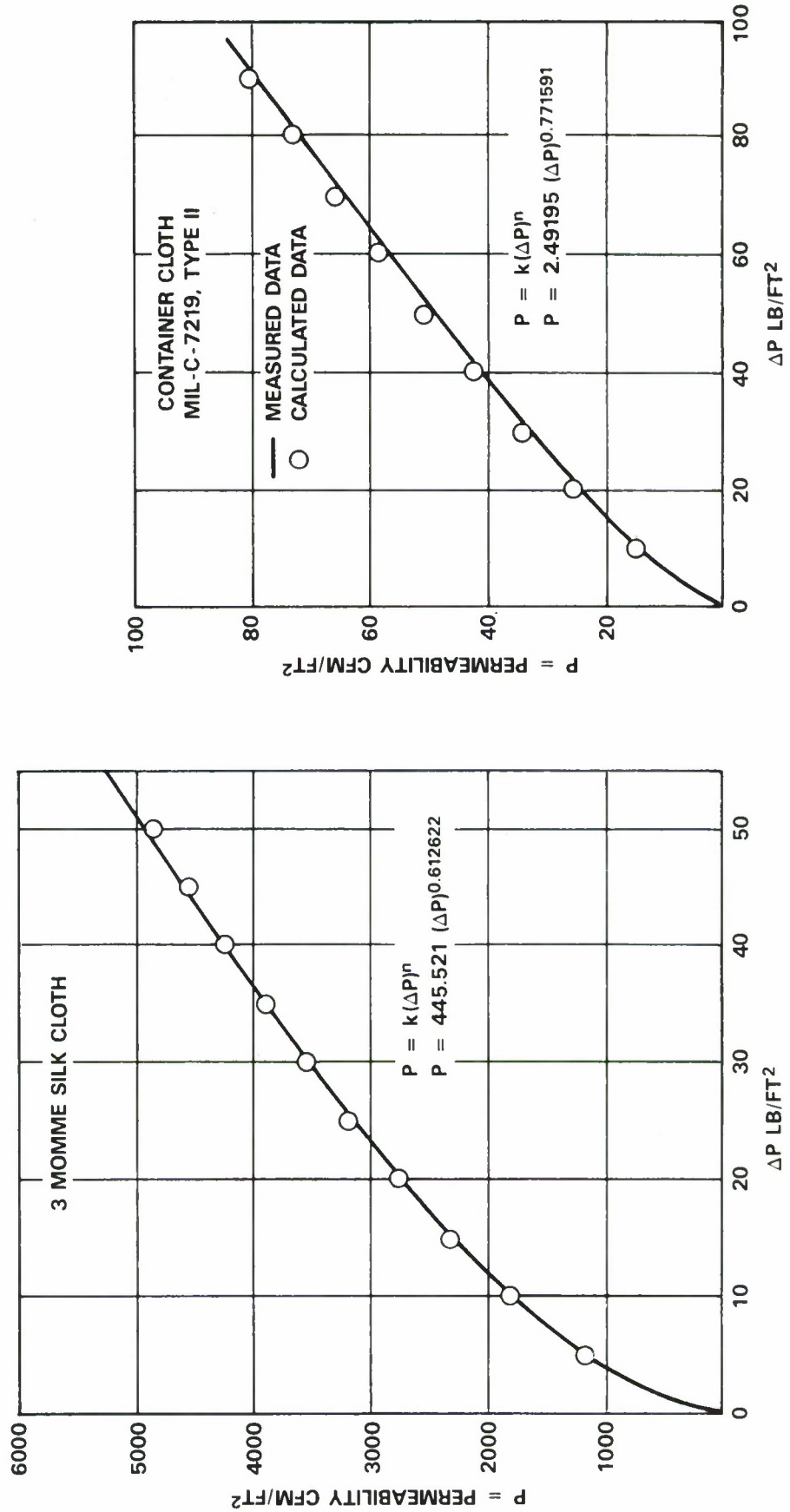

FIGURE 16. COMPARISON OF MEASURED AND CALCULATED PERMEABILITY FOR RELATIVELY PERMEABLE AND IMPERMEABLE CLOTHS

Comparison of the mass flow ratio and previously published effective porosity data is shown in Figure 17. The effects of altitude and velocity on the mass flow ratio are presented in Figures 18 and 19 for constant velocity and constant altitude. The decrease of cloth permeability with altitude is evident. The reduced outflow rate causes the canopy to inflate more quickly as the altitude is raised.

The relationship of k, n, and altitude on the inflation reference time is illustrated in Figure 20.

The permeability constants "k" and "n" can be determined from the permeability-pressure differential data as obtained from an instrument such as a Frazier Permeameter. Two data points, "A" and "B," are selected in such a manner that point "A" is in a low-pressure zone below the knee of the curve, and point "B" is located in the upper end of the high-pressure zone, as shown in Figure 21.

Two measurements at 1/2 inch of water and 20 inches of water appear to be good data points if both are available on the same sample. Substituting the data from points "A" and "B" into $P = k(\Delta P)^n$:

$$n = \frac{\ln\left(\frac{P_B}{P_A}\right)}{\ln\left(\frac{\Delta P_B}{\Delta P_A}\right)} \tag{28}$$

$$k = \frac{P_A}{(\Delta P_A)^n} = \frac{P_B}{(\Delta P_B)^n} \tag{29}$$

Another method of determining k and n is to adapt a least squares fit through all of the cloth rate of airflow - pressure differential measurements. A true average value of k and n in any given parachute requires a large number of permeameter rate of airflow tests due to the variation of the woven cloth airflow rates. Their values may also vary for different parachutes in the same lot. This is most likely one of the causes of performance variations for similar test conditions.

PARACHUTE AVERAGE PRESSURE COEFFICIENT

The average pressure coefficient, C_{pav}, of a parachute is the parachute drag coefficient referenced to the projected canopy area.

The average pressure coefficient for the steady-state parachute was determined as follows:

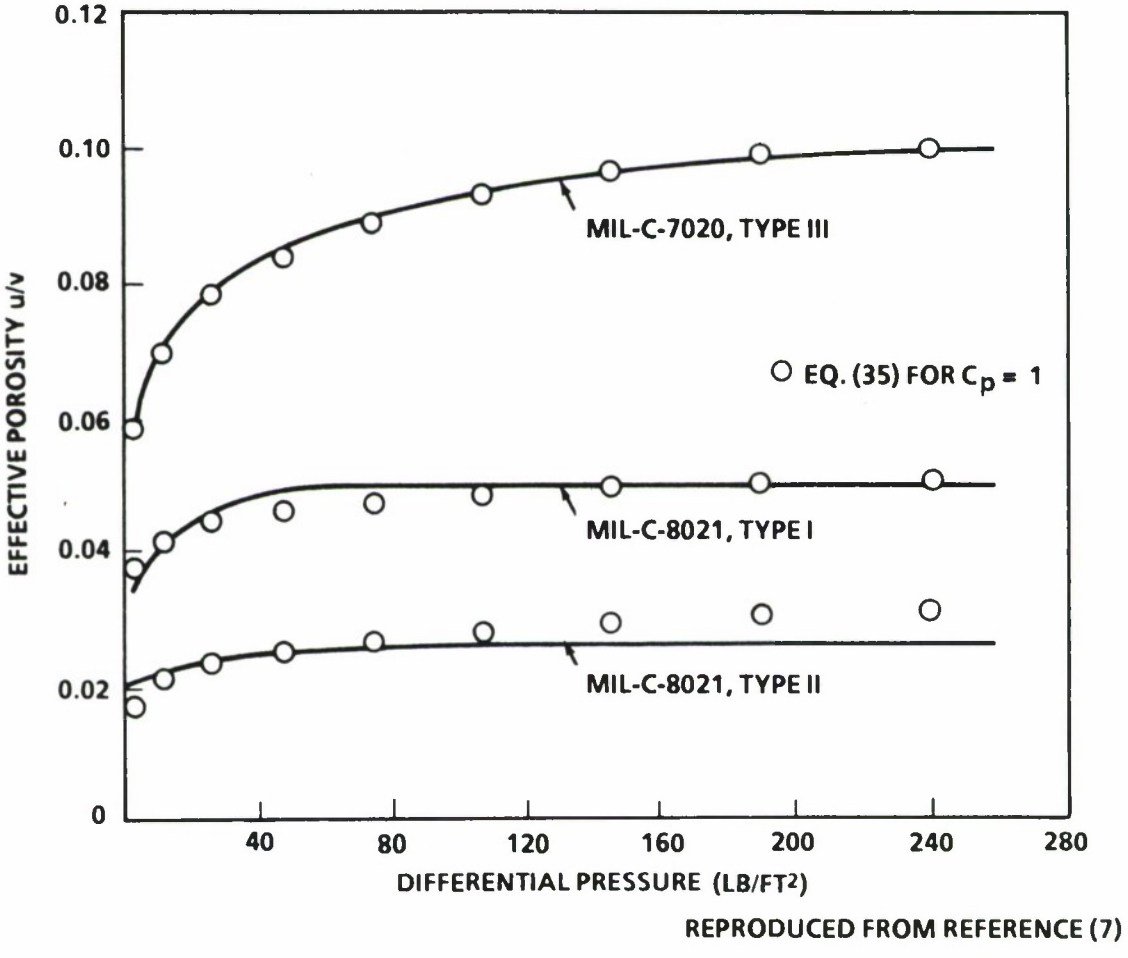

FIGURE 17. THE EFFECTIVE POROSITY OF PARACHUTE MATERIALS VERSUS DIFFERENTIAL PRESSURE

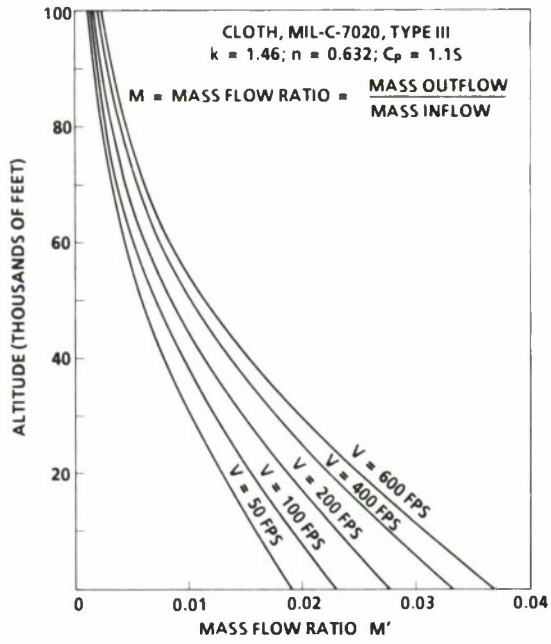

FIGURE 18. EFFECT OF ALTITUDE ON MASS FLOW RATIO AT CONSTANT VELOCITY

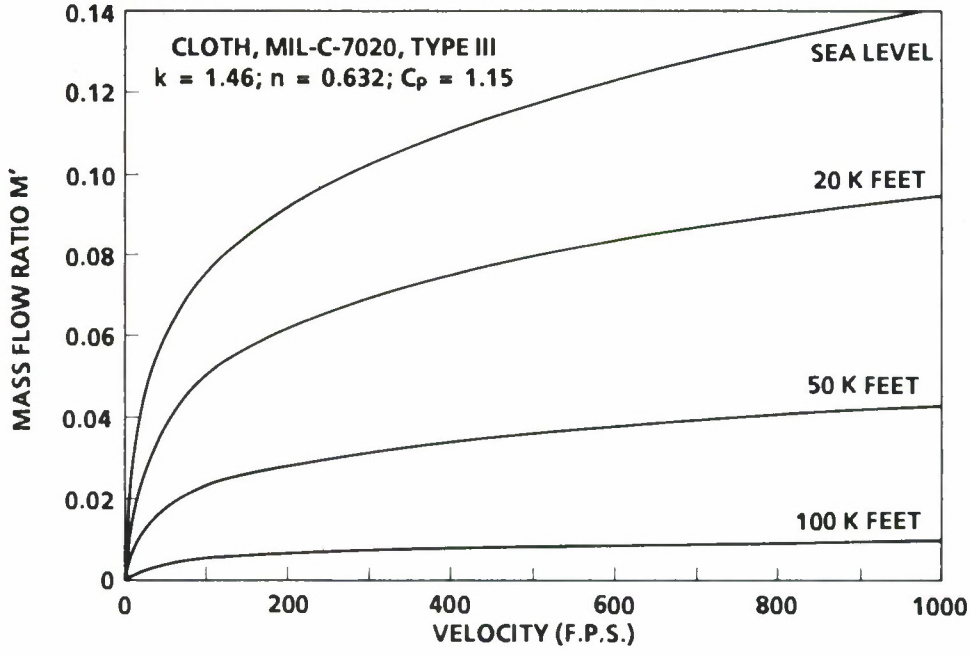

FIGURE 19. EFFECT OF VELOCITY ON MASS FLOW RATIO AT CONSTANT DENSITY

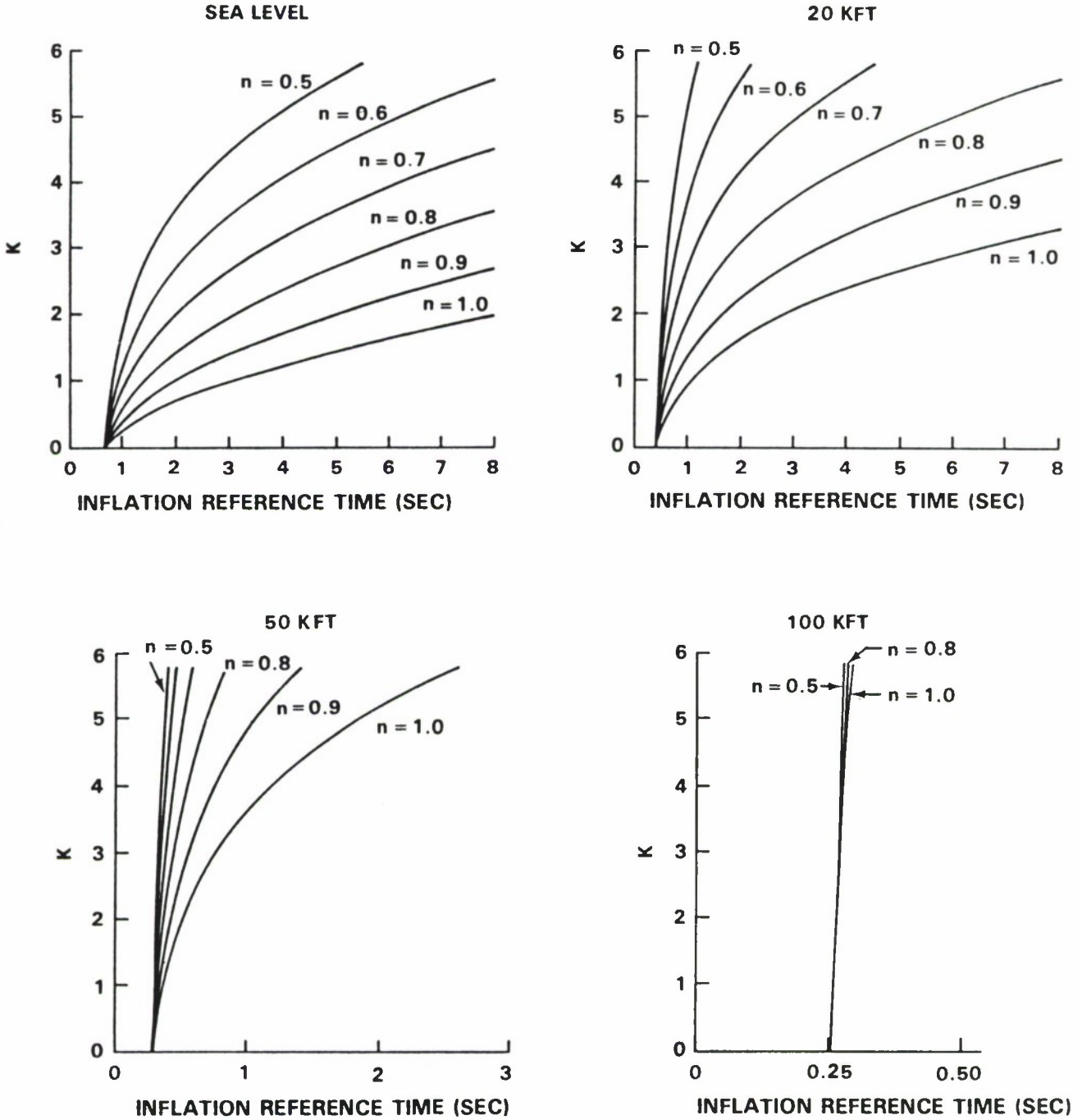

CLOTH	k	n
MIL-C-7020, TYPE III	1.46042	0.63246
MIL-C-8021, TYPE I	0.99469	0.57403
MIL-C-8021, TYPE II	0.44117	0.60492

FIGURE 20. EFFECT OF CANOPY CLOTH CONSTANTS "k" AND "n" ON THE PARACHUTE INFLATION REFERENCE TIME "T_O"

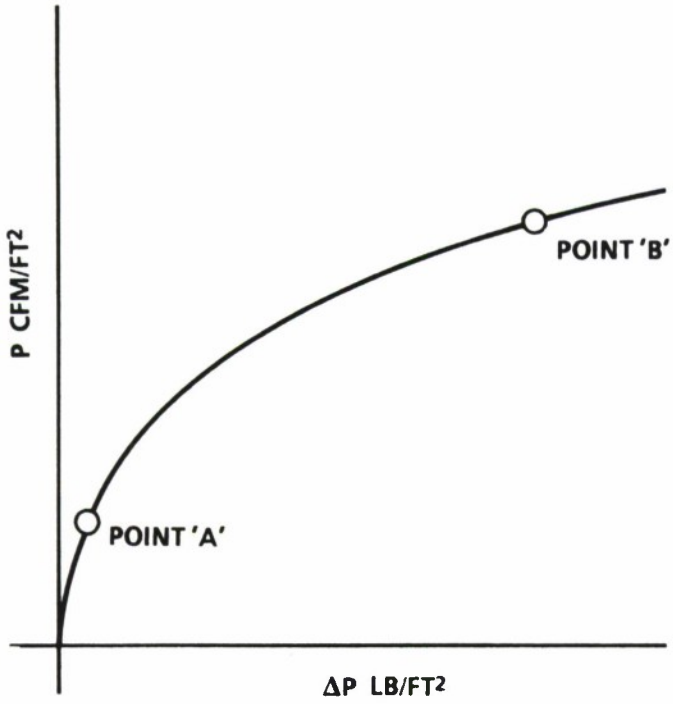

FIGURE 21. LOCATION OF DATA POINTS FOR DETERMINATION OF "k" AND "n"

The steady-state drag force, in a wind tunnel for example, may be written

$$F = q C_D S_o \tag{30}$$

but it may also be written

$$F = \Delta P_{av} S_p \tag{30a}$$

where S_p is the projected area of the inflated canopy and $\overline{\Delta P}_{av}$ is the average pressure differential acting on S_p.

$$\Delta P_{av} S_p = F = q C_D S_o$$

$$C_{p_{av}} = \frac{\Delta P_{av}}{q} = \frac{C_D S_o}{S_p}$$

$$S_o = \frac{\pi}{4} D_o^2$$

$$S_p = \frac{\pi}{4} D_p^2$$

$$\frac{S_o}{S_p} = \left(\frac{D_o}{D_p}\right)^2 = \frac{1}{\left(\frac{D_p}{D_o}\right)^2}$$

$$C_{p_{av}} = \frac{C_D}{\left(\frac{D_p}{D_o}\right)^2}$$

ratios of D_p/D_o from Reference 6 are presented in Table 2 for several types of parachutes.

TABLE 2. RANGE OF AVERAGE STEADY-STATE CANOPY PRESSURE COEFFICIENTS

PARACHUTE TYPE	C_D RANGE	D_p/D_o RANGE	C_{pav} RANGE
FLAT CIRCULAR	0.75 0.80	0.70 0.67	1.531 1.782
EXTENDED SKIRT	0.78 0.87	0.70 0.66	1.592 1.997
CROSS	0.60 0.78	0.72 0.66	1.157 1.791

For a flat circular parachute with a $C_D = 0.75$ and $D_p/D_o = 0.67$

$$C_{p_{av}} = \frac{0.75}{(0.67)^2}$$

$$C_{p_{av}} = 1.671$$

The inflation geometry as a function of t/t_o is constant with altitude. It can be deduced from this that if the inflating geometry is independent of altitude, the force distribution which causes the geometry to develop must also be independent of altitude. These forces come from the pressure distribution along the gore panel. Therefore, at any given t/t_o a definite, repeatable pressure distribution exists which varies with t/t_o, but is constant for all altitudes and the C_{pav} is constant with altitude. Figure 22 gives the effect of varying the magnitude of the average pressure coefficient at altitudes from sea level to 100,000 feet. At sea level the magnitude of the average pressure coefficient affects the value of the inflation reference time. The effect is magnified as the exponent "n" increases. As the altitude increases the particular magnitude of the average pressure coefficient is less significant.

Table 2 presented the range of C_{pav} that can be expected for a definite parachute type. Figure 22 presents the effects of the variation of the average

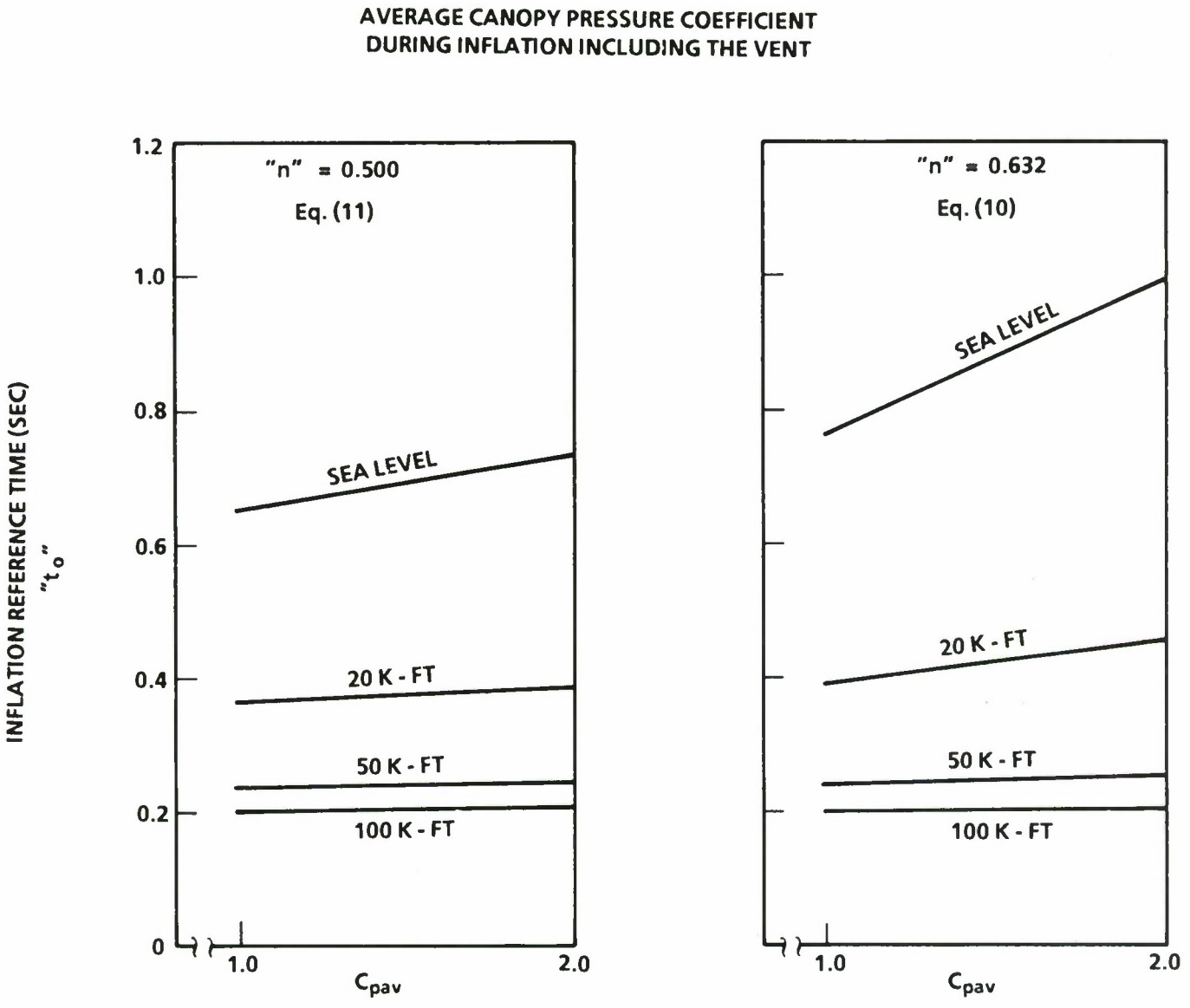

FIGURE 22. EFFECT OF PRESSURE COEFFICIENT AND ALTITUDE ON THE UNFOLDING TIME

pressure coefficient on the inflation reference time for a given parachute system. The largest inflation reference time variation occurs at sea level. As the altitude is raised the variation decreases to a constant time value. As n approaches 1 the noted effects are accentuated.

The Air Force Flight Dynamics Laboratory conducted field tests of a 28-foot (D_o) Solid Flat Circular Parachute (SFCP) system at altitudes of 6,000, 13,000, and 21,000 feet. A result of these tests was the demonstration of the repeatability of the canopy projected area to surface area ratio at all test altitudes. With the data of Figure 1, the average pressure coefficients for the 28-foot SFCP can be estimated during the inflation process.

$$C_{p_{av}} = \frac{C_D S}{S_p} \tag{31}$$

$$C_D S = C_D S_o \left[(1-\eta) \left(\frac{t}{t_o} \right)^3 + \eta \right]^2$$

$$C_{p_{av}} = \frac{C_D}{S_p/S_o} \left[(1-\eta) \left(\frac{t}{t_o} \right)^3 + \eta \right]^2$$

for $0 \leq t/t_o \leq 0.3$

$$C_{p_{av}} = \frac{C_D \left[(1-\eta) \left(\frac{t}{t_o} \right)^3 + \eta \right]^2}{0.0024 + 0.07843 \left(\frac{t}{t_o} \right)} \tag{32}$$

for $0.3 \leq t/t_o \leq 1.0$

$$C_{p_{av}} = \frac{C_D \left[(1-\eta) \left(\frac{t}{t_o} \right)^3 + \eta \right]^2}{0.0117 + 0.0034 \, (118.4)^{t/t_o}} \tag{33}$$

when $\eta = \tau = 0$

for $0 \leq t/t_o \leq 0.3$

$$C_{p_{av}} = \frac{C_D \left(\frac{t}{t_o} \right)^6}{0.0024 + 0.07843 \left(\frac{t}{t_o} \right)} \tag{34}$$

for $0.3 \leq t/t_o \leq 1.0$

$$C_{p_{av}} = \frac{C_D \left(\frac{t}{t_o}\right)^6}{0.0117 + 0.0034\,(118.4)^{t/t_o}} \tag{35}$$

Figure 23 shows the estimated variation of C_p during inflation for the following conditions: $C_D = 0.75$; $\eta = 0.0024$; $t_o = t_f$; and the two variations of S_p/S_o as a function of t/t_f in Figure 1.

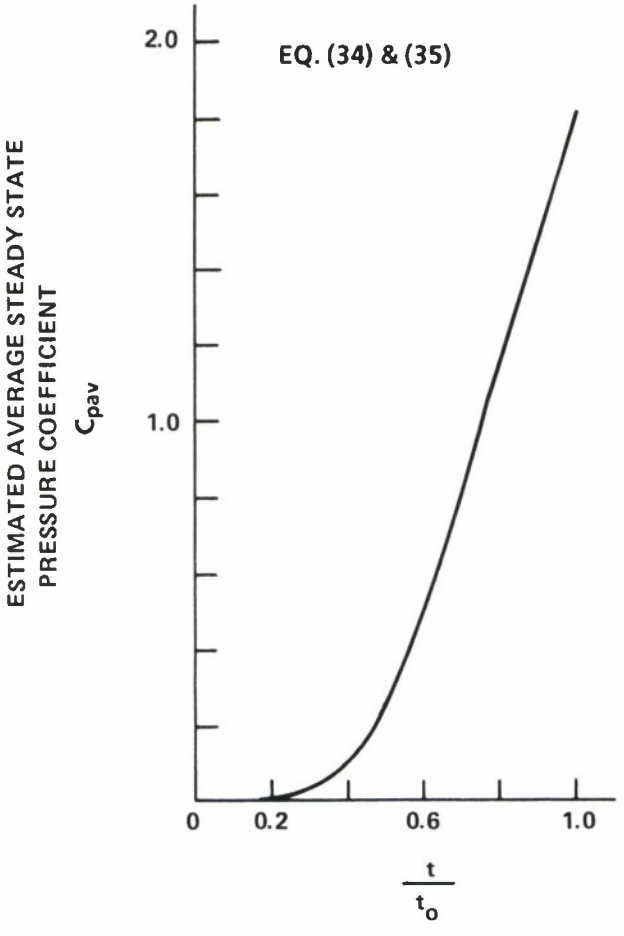

FIGURE 23. ESTIMATED STEADY-STATE AVERAGE PRESSURE COEFFICIENT FOR THE INFLATING 28-FOOT (D_O) SOLID FLAT CIRCULAR PARACHUTE OF FIGURE 1

When calculating the inflation reference time of solid cloth parachutes, I have achieved good results using a constant value of steady-state average pressure coefficient in the inflation time equations.

CONCLUSIONS

1. An inflating parachute's transient geometric shapes, volumes, and drag areas are independent of altitude, velocity, and system mass restraints.

2. The parachute inflation distance ($V_S t_o$) axiom has been verified and demonstrated to be a constant which is a function of altitude.

3. The parachute inflation time-opening shock force axiom has been demonstrated to appear to be true, but really is not.

4. The opening shock force of a given parachute system is determined by the initial design requirements, type of parachute, and canopy airflow, as well as the operational altitude, velocity, and trajectory deployment angle.

5. The inflation reference times of solid cloth parachutes vary as the weight-to-drag-area ratio increases.

6. The inflation distance formula (12) shows that the performance depends on system area ratios, mass ratios, canopy airflow, and the Ballistic Mass Ratio scale parameter per foot of length.

7. The inflation distance formula effective mouth area term yields some clues about critical velocity.

8. Inflation time formulas which require the line stretch velocity to be raised to the 0.9 power, can achieve the same result by dividing the line stretch velocity by 2 and setting the exponent of V_s to unity.

9. Equation (11) shows good agreement with the empirical inflation time in the low altitude regime, and shows a reduction in inflation time as the altitude rises.

10. The reduction of inflation reference time and distance is due to the lowering of air density as the altitude increases.

11. The cloth rate of airflow formula is suitable to high rates of airflow and low rates of airflow cloths.

12. The mass flow ratio, M', is similar to effective porosity, C.

13. At low altitudes the particular value of the cloth airflow constants have a considerable effect on the inflation reference time. As the altitude increases, the effect of k and n on the inflation reference time is reduced. At an altitude of 100,000 feet, the time variation is minimal.

14. The average pressure coefficient of a parachute is the parachute drag coefficient based upon the projected area of the inflated canopy. The intermediate

instantaneous average pressure coefficients can be determined if the instantaneous drag force and projected area are known.

15. The effect of the average pressure coefficient on the variation of the inflation reference time is most pronounced at sea level and least pronounced at high altitude. As the exponent n increases from 0.5, the effects are intensified.

REFERENCES

1. Ludtke, W.P., *Observations on Parachute Scale Factors for Modeling Parachute Deployment and Steady-State Performance*, NSWC/WOL TR 78-189.

2. Ludtke, W.P., *Alternate Altitude Testing of Solid Cloth Parachute Systems*, NSWC TR 85-24.

3. Ludtke, W.P., *Notes on a Generic Parachute Opening Force Analysis*, NSWC TR 86-142.

4. Ludtke, W.P., *Notes on a Parachute Opening Force Analysis Applied to a Vertical Toward-the-Earth Trajectory*, NSWC TR 87-96.

5. Ludtke, W.P., *Notes on a Theoretical Parachute Opening Force Analysis Applied to a General Trajectory*, NSWC TR 88-6.

6. Air Force Flight Dynamics Laboratory, *Recovery Systems Design Guide*, AFFDL-TR-78-151.

7. Knacke, T., "Lecture Notes from the Helmut G. Heinrich Short Course on Decelerator Systems Technology." Presented at the Sandia National Laboratories, July 1985.

Appendix A

AIAA Paper No. 73-477

A TECHNIQUE FOR THE CALCULATION OF THE OPENING-SHOCK FORCES FOR SEVERAL TYPES OF SOLID CLOTH PARACHUTES

by
W. P. LUDTKE
Naval Ordnance Laboratory
Silver Spring, Maryland

AIAA 4th Aerodynamic Deceleration Systems Conference

PALM SPRINGS, CALIFORNIA / MAY 21-23, 1973

A TECHNIQUE FOR THE CALCULATION OF THE OPENING-SHOCK FORCES FOR SEVERAL TYPES OF SOLID CLOTH PARACHUTES

W. P. Ludtke
Naval Ordnance Laboratory
Silver Spring, Maryland

Abstract

An analytical method of calculating parachute opening-shock forces based upon wind-tunnel derived drag area time signatures of several solid cloth parachute types in conjunction with a scale factor and retardation system steady-state parameters has been developed. Methods of analyzing the inflation time, geometry, cloth airflow properties and materials elasticity are included. The effects of mass ratio and altitude on the magnitude and time of occurrence of the maximum opening shock are consistent with observed field test phenomena.

I. Introduction

In 1965, the Naval Ordnance Laboratory (NOL) was engaged in a project which utilized a 35-foot-diameter, 10-percent extended-skirt parachute (type T-10) as the second stage of a retardation system for a 250-pound payload. Deployment of the T-10 parachute was to be accomplished at an altitude of 100,000 feet. In this rarefied atmosphere, the problem was to determine the second stage deployment conditions for successful operation. A search of available field test information indicated a lack of data on the use of solid cloth parachutes at altitudes above 30,000 feet.

The approach to this problem was as follows: Utilizing existing wind-tunnel data, low-altitude field test data, and reasonable assumptions, a unique engineering approach to the inflation time and opening-shock problem was evolved that provided satisfactory results. Basically, the method combines a wind-tunnel derived drag area ratio signature as a function of deployment time with a scale factor and Newton's second law of motion to analyze the velocity and force profiles during deployment. The parachute deployment sequence is divided into two phases. The first phase, called "unfolding phase," where the canopy is undergoing changes in shape, is considered to be inelastic as the parachute inflates initially to its steady-state aerodynamic size for the first time. At this point, the "elastic phase" is entered where it is considered that the elasticity of the parachute materials enters the problem and resists the applied forces until the canopy has reached full inflation.

The developed equations are in agreement with the observed performance of solid cloth parachutes in the field, such as the decrease of inflation time as altitude increases, effects of altitude on opening-shock force, finite and infinite mass operation, and inflation distance.

II. Development of Velocity Ratio and Force Ratio Equations During the Unfolding Phase of Parachute Deployment

The parachute deployment would take place in a horizontal attitude in accordance with Newton's second law of motion.

$$\Sigma F = ma$$

$$-\frac{1}{2}\rho V^2 C_D S = \frac{W}{g}\frac{dV}{dt}$$

It was recognized that other factors, such as included air mass, apparent mass, and their derivatives, also contribute forces acting on the system. Since definition of these parameters was difficult, the analysis was conducted in the simplified form shown above. Comparison of calculated results and test results indicated that the omitted terms have a small effect.

$$\int_o^t C_D S\,dt = \frac{-2W}{\rho g}\int_{V_s}^{V}\frac{dV}{V^2} \qquad (1)$$

Multiplying the right-hand side of equation (1) by

$$1 = \frac{V_s t_o C_D S_c}{V_s t_o C_D S_o}$$

and rearranging

$$\frac{1}{t_o}\int_o^t \frac{C_D S}{C_D S_o}\,dt$$

$$= \frac{-2W}{\rho g V_s t_o C_D S_o} V_s \int_{V_s}^{V}\frac{dV}{V^2} \qquad (2)$$

In order to integrate the left-hand term of equation (2), the drag area ratio must be defined for the type of parachute under

analysis as a function of deployment reference time, t_o.

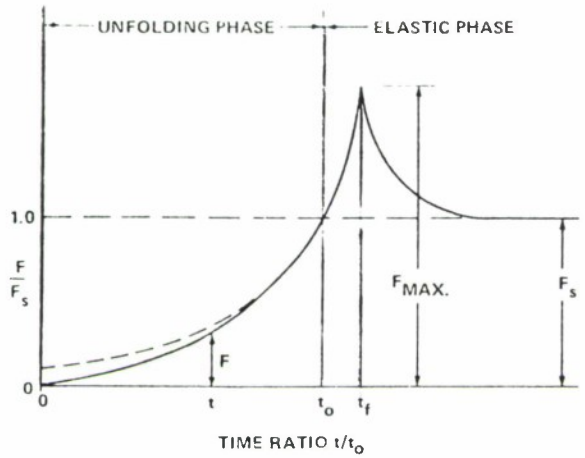

FIG. 1 TYPICAL INFINITE MASS FORCE-TIME HISTORY OF A SOLID CLOTH PARACHUTE IN A WIND TUNNEL

Figure 1 illustrates a typical solid cloth parachute wind-tunnel infinite mass force-time history after snatch. In infinite mass deployment, the maximum size and maximum shock force occur at the time of full inflation, t_f. However, t_f is inappropriate for analysis since it is dependent upon the applied load, structural strength, and materials elasticity. The reference time, t_o, where the parachute has attained its steady-state aerodynamic size for the first time, is used as the basis for performance calculations.

At any instant during the unfolding phase, the force ratio F/F_s can be determined as a function of the time ratio, t/t_o.

$$F = \frac{1}{2}\rho V^2 C_D S$$

$$F_s = \frac{1}{2}\rho V_s^2 C_D S_o$$

Since the wind-tunnel velocity and density are constant during infinite mass deployment

$$\frac{F}{F_s} = \frac{C_D S}{C_D S_o}$$

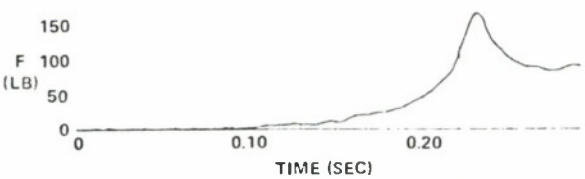

FIG. 2 TYPICAL FORCE-TIME CURVE FOR A SOLID FLAT PARACHUTE UNOER INFINITE MASS CONOITIONS.

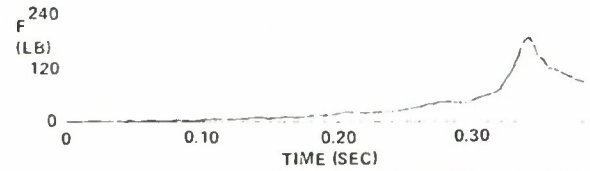

REPRODUCED FROM REFERENCE (1)

FIG. 3 TYPICAL FORCE-TIME CURVE FOR A 10% EXTENDED SKIRT PARACHUTE UNOER INFINITE MASS CONOITIONS.

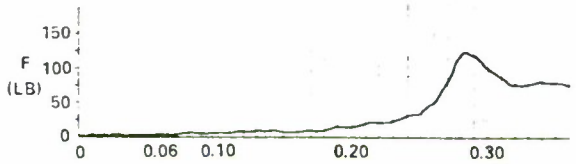

REPROOUCED FROM REFERENCE (1)

FIG. 4 TYPICAL FORCE-TIME CURVE FOR A PERSONNEL GUIOE SURFACE PARACHUTE UNOER INFINITE MASS CONOITIONS

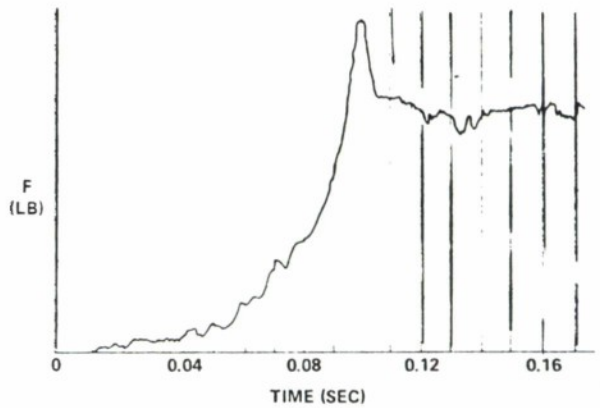

FIG. 5 TYPICAL FORCE-TIME SIGNATURE FOR THE ELLIPTICAL PARACHUTE UNDER INFINITE MASS CONDITIONS

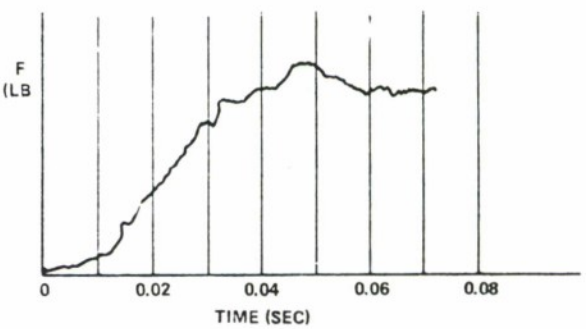

FIG. 6 TYPICAL FORCE-TIME SIGNATURE FOR THE RING SLOT PARACHUTE 20% GEOMETRIC POROSITY UNDER INFINITE MASS CONOITIONS

Infinite mass opening-shock signatures of several types of parachutes are presented in Figures 2 through 6. Analysis of these signatures using the force ratio, F/F_s, - time ratio, t/t_o, technique indicated a similarity in the performance of the various solid cloth types of

parachutes which were examined. The geometrically porous ring slot parachute displayed a completely different signature, as was expected. These data are illustrated in Figure 7. If an initial boundary

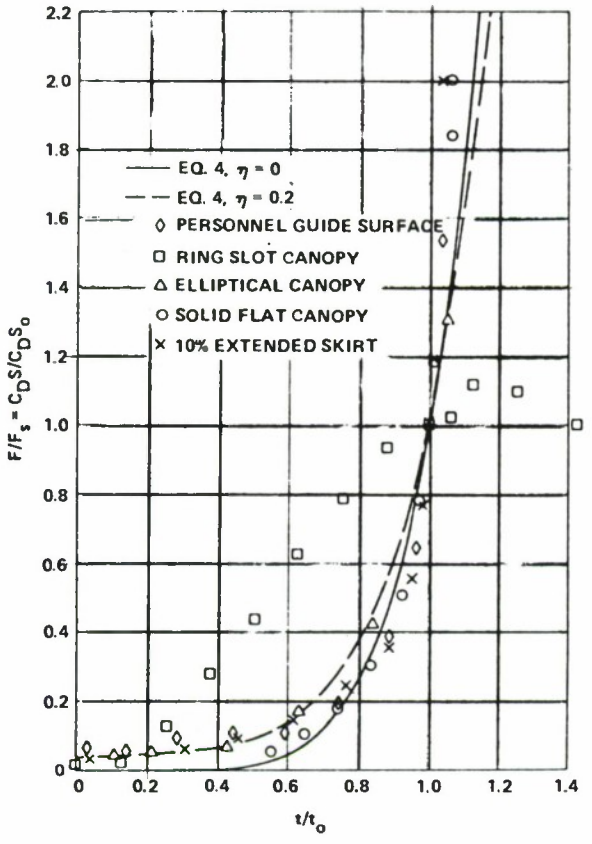

FIG. 7 DRAG AREA RATIO VS. TIME RATIO

condition of $C_DS/C_DS_o = 0$ at time $t/t_o = 0$ is assumed, then, the data can be approximated by fitting a curve of the form

$$\frac{C_DS}{C_DS_o} = \left(\frac{t}{t_o}\right)^6 \qquad (3)$$

A more realistic drag area ratio expression was determined which includes the effect of initial area at line stretch.

$$\frac{C_DS}{C_DS_o} = \left[\left(1-\eta\right)\left(\frac{t}{t_o}\right)^3 + \eta\right]^2 \qquad (4)$$

where η is the ratio of the projected mouth area at line stretch to the steady-state projected frontal area. Expanding equation (4)

$$\frac{C_DS}{C_DS_o} = \left(1-\eta\right)^2\left(\frac{t}{t_o}\right)^6 + 2\eta\left(1-\eta\right)\left(\frac{t}{t_o}\right)^3 + \eta^2 \qquad (5)$$

At the time that equation (5) was ascertained, it suggested that the geometry of the deploying parachute was independent of density and velocity. It was also postulated that although this expression had been determined for the infinite mass condition, it would also be true for the finite mass case. This phenomenon has since been independently observed and confirmed by Berndt and De Weese in reference (2).

Since the drag area ratio was determined from actual parachute deployments, it was assumed that the effects of apparent mass and included mass on the deployment force history were accommodated.

The right-hand term of equation (2) contains the expression

$$\frac{2W}{\rho g V_s t_o C_D S_o} = M \qquad (6)$$

This term can be visualized as shown in Figure 8 to be a ratio of the retarded mass (including the parachute) to an associated mass of atmosphere contained in a right circular cylinder which is generated by moving an inflated parachute of area C_DS_o for a distance equal to the product of V_st_o through an atmosphere of density, ρ.

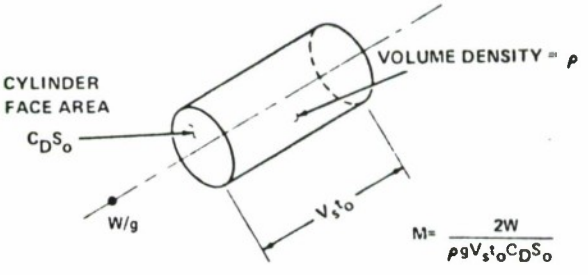

FIG. 8 VISUALIZATION OF THE MASS RATIO CONCEPT

The mass ratio, M, is the scale factor which controls the velocity and force profiles during parachute deployment. Substituting M and C_DS/C_DS_o into equation (2), integrating, and solving for V/V_s

$$\frac{V}{V_s} = \frac{1}{1+\frac{1}{M}\left[\frac{(1-\eta)^2}{7}\left(\frac{t}{t_o}\right)^7 + \frac{\eta(1-\eta)}{2}\left(\frac{t}{t_o}\right)^4 + \eta^2\frac{t}{t_o}\right]} \qquad (7)$$

The instantaneous shock factor is defined as

$$x_i = \frac{F}{F_s} = \frac{\frac{1}{2}\rho V^2 C_D S}{\frac{1}{2}\rho V_s^2 C_D S_o}$$

If the altitude variation during deployment is small, then, the density may be considered as constant

$$x_i = \frac{C_D S}{C_D S_o}\left(\frac{V}{V_s}\right)^2$$

from equations (5) and (7)

$$x_i = \frac{(1-\eta)^2\left(\frac{t}{t_o}\right)^6 + 2\eta(1-\eta)\left(\frac{t}{t_o}\right)^3 + \eta^2}{\left[1 + \frac{1}{M}\left[\frac{(1-\eta)^2}{7}\left(\frac{t}{t_o}\right)^7 + \frac{\eta(1-\eta)}{2}\left(\frac{t}{t_o}\right)^4 + \eta^2\frac{t}{t_o}\right]\right]^2} \quad (8)$$

III. Maximum Shock Force and Time of Occurrence During the Unfolding Phase

The time of occurrence of the maximum instantaneous shock factor, x_i, is difficult to determine for the general case. However, for $\eta = 0$, the maximum shock factor and time of occurrence are readily calculated. For $\eta = 0$

$$x_i = \frac{\left(\frac{t}{t_o}\right)^6}{\left[1 + \frac{1}{7M}\left(\frac{t}{t_o}\right)^7\right]^2}$$

Setting the derivative of x_i with respect to time equal to zero and solving for t/t_o at $x_{i\,max}$

$$\left(\frac{t}{t_o}\right)_{@\, x_{i\,max}} = \left(\frac{21M}{4}\right)^{\frac{1}{7}} \quad (9)$$

and the maximum shock factor is

$$x_{i\,max} = \frac{16}{49}\left(\frac{21M}{4}\right)^{\frac{6}{7}} \quad (10)$$

Equations (9) and (10) are valid for values of $M \leq \frac{4}{21}$ (0.19), since for larger values of M, the maximum shock force occurs in the elastic phase of inflation.

Figures 9 and 10 illustrate the velocity and force profiles generated from equations (7) and (8) for initial projected area ratios of $\eta = 0$, and 0.2 with various mass ratios.

IV. Methods for Calculation of the Reference Time, t_o

The ratio concept is an ideal method to analyze the effects of the various parameters on the velocity and force profiles of the opening parachutes; however, a means of calculating t_o is required before specific values can be computed. Methods for computing the varying mass flow into the inflating canopy mouth, the varying mass flow out through the varying inflated canopy surface area, and the volume of air, V_o, which must be collected during the inflation process are required.

Figure 11 represents a solid cloth-type parachute canopy at some instant during inflation. At any given instant, the parachute drag area is proportional to the maximum inflated diameter. Also, the maximum diameter in conjunction with the suspension lines determines the inflow mouth area (A-A) and the pressurized canopy area (B-B-B). This observation provided the basis for the following assumptions. The actual canopy shape is of minor importance.

a. The ratio of the instantaneous mouth inlet area to the steady-state mouth area is in the same ratio as the instantaneous drag area.

$$\frac{A_M}{A_{Mo}} = \frac{C_D S}{C_D S_o}$$

b. The ratio of the instantaneous pressurized cloth surface area to the canopy surface area is in the same ratio as the instantaneous drag area.

$$\frac{S}{S_o} = \frac{C_D S}{C_D S_o}$$

c. Since the suspension lines in the unpressurized area of the canopy are straight, a pressure differential has not developed, and, therefore, the net airflow in this zone is zero.

Based on the foregoing assumptions, the mass flow equation can be written

$$dm = m\ \text{inflow} - m\ \text{outflow}$$

$$\rho\frac{dV}{dt} = \rho V A_M - \rho A_s P$$

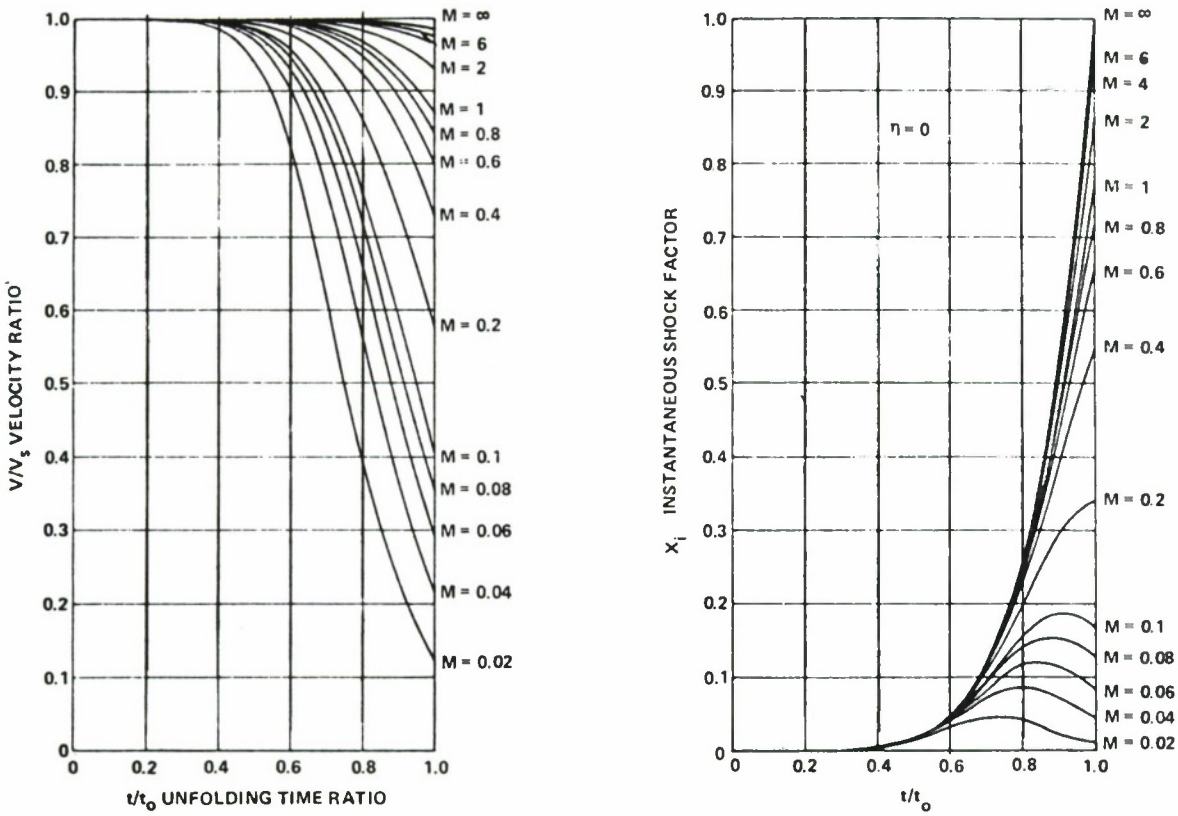

FIG. 9 EFFECT OF INITIAL AREA AND MASS RATIO ON THE SHOCK FACTOR AND VELOCITY RATIO DURING THE UNFOLDING PHASE FOR $\eta = 0$.

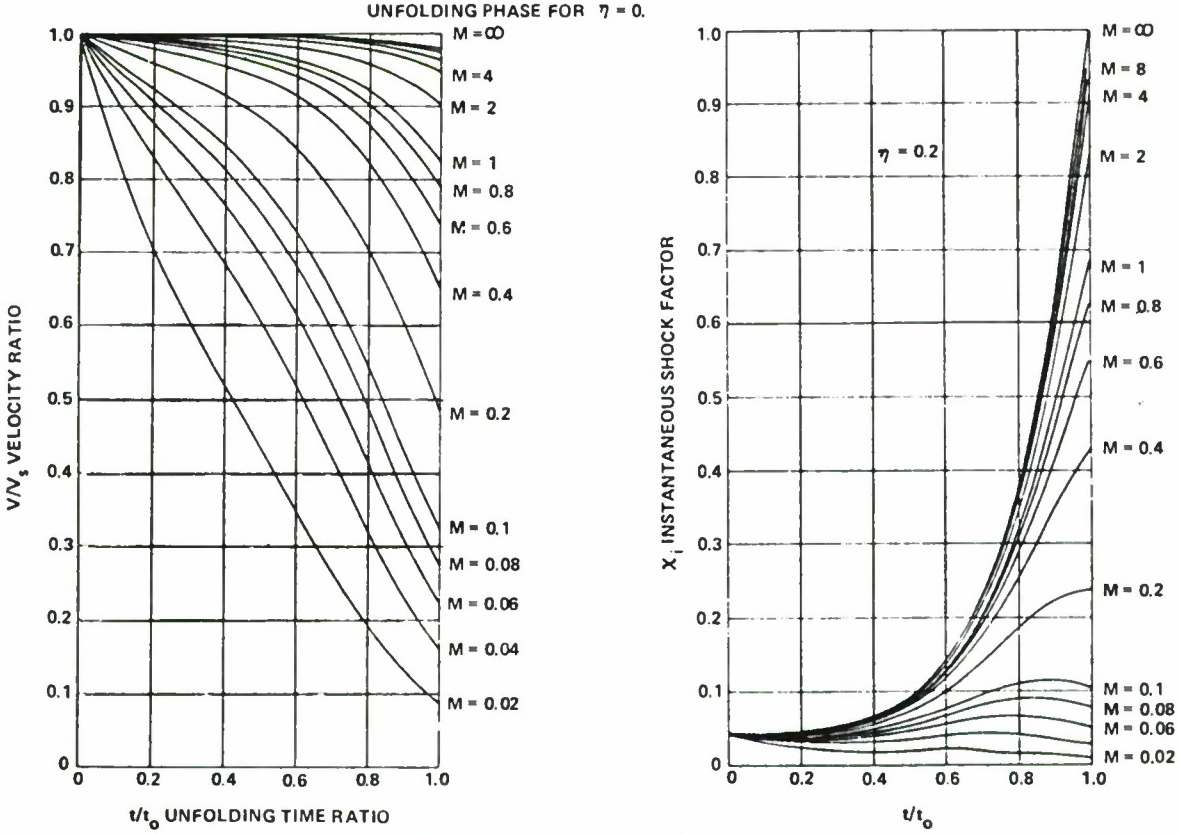

FIG. 10 EFFECT OF INITIAL AREA AND MASS RATIO ON THE SHOCK FACTOR AND VELOCITY RATIO DURING THE UNFOLDING PHASE FOR $\eta = 0.2$

$$\rho \frac{dV}{dt} = \rho V A_{Mo} \frac{C_D S}{C_D S_o} - \rho A_{So} \frac{C_D S}{C_D S_o} P \qquad (11)$$

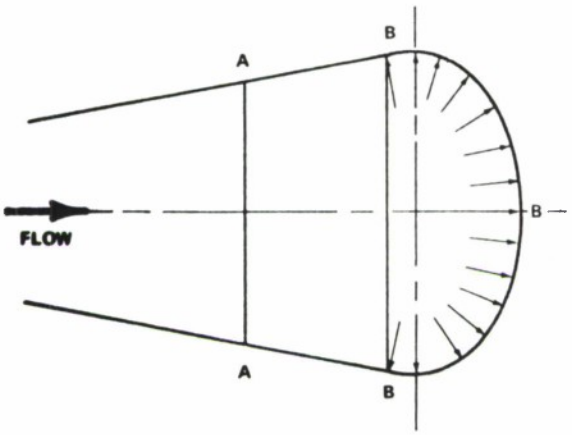

FIG. 11 PARTIALLY INFLATED PARACHUTE CANOPY

From equation (3)

$$\frac{C_D S}{C_D S_o} = \left(\frac{t}{t_o}\right)^6 \quad ; \text{ for } \eta = 0$$

From equation (7)

$$V = \frac{V_s}{1 + \frac{1}{7M}\left(\frac{t}{t_o}\right)^7} \quad ; \eta = 0$$

From equation (26)

$$P = k\left(\frac{C_P \rho}{2}\right)^n V^{2n}$$

$$\int_o^{\underline{V}_o} d\underline{V} = A_{Mo} V_s \int_o^{t_o} \frac{\left(\frac{t}{t_o}\right)^6}{1 + \frac{1}{7M}\left(\frac{t}{t_o}\right)^7} dt$$

$$-A_{So} k \left(\frac{C_P \rho}{2}\right)^n \int_o^{t_o} \left(\frac{t}{t_o}\right)^6 \left[\frac{V_s}{1 + \frac{1}{7M}\left(\frac{t}{t_o}\right)^7}\right]^{2n} dt \qquad (12)$$

Integrating:

$$\underline{V}_o = A_{Mo} V_s t_o M \ln\left[1 + \frac{1}{7M}\right]$$

$$-A_{So} k \left(\frac{C_P \rho}{2}\right)^n \int_o^{t_o} \left(\frac{t}{t_o}\right)^6 \left[\frac{V_s}{1 + \frac{1}{7M}\left(\frac{t}{t_o}\right)^7}\right]^{2n} dt \qquad (13)$$

Measured values of n indicate a data range from 0.574 through 0.771. A convenient solution to the reference time equation evolves when n is assigned a value of 1/2. Integrating equation (13) and using

$$V_s t_o M = \frac{2W}{g\rho C_D S_o}$$

$$\text{LET } K_1 = \frac{g\rho \underline{V}_o}{2W}\left[\frac{C_D S_o}{A_{Mo} - A_{So} k\left(\frac{C_P \rho}{2}\right)^{1/2}}\right]$$

$$t_o = \frac{14W}{g\rho V_s C_D S_o}\left[e^{K_1} - 1\right] \qquad (14)$$

Equation (14) expresses the unfolding reference time, t_o, in terms of mass, altitude, snatch velocity, airflow characteristics of the cloth, and the steady-state parachute geometry. Note that the term $g\rho\underline{V}_o/W$ is the ratio of the included air mass to the mass of the retarded hardware. Multiplying both sides of equation (14) by V_s demonstrates that

$V_s t_o$ = a constant which is a function of altitude

Figures 12 and 13 indicate the parachute unfolding time and unfolding distance for values of n = 1/2 and n = 0.63246. Note the variation and convergence with rising altitude. The opening-shock force is strongly influenced by the inflation time. Because of this, the

value of t_o calculated by using a realistic value of n should be used in the lower atmosphere.

As an example of this method of opening-shock analysis, let us examine the effect of altitude on the opening-shock force of a T-10-type parachute retarding a 200-pound weight from a snatch velocity of V_S = 400 feet per second at sea level. Conditions of constant velocity and constant dynamic pressure are investigated. The results are presented in Figure 14. At low altitudes, the opening-shock force is less than the steady-state drag force; however, as altitude rises, the opening shock eventually exceeds the steady-state drag force at some altitude. This trend is in agreement with field test observations.

V. Correction of t_o for Initial Area Effects

The unfolding reference time, t_o, calculated by the previous methods assumes that the parachute inflates from zero drag area. In reality, a parachute has a drag area at the beginning of inflation. Once t_o has been calculated, a correction can be applied, based upon what is known about the initial conditions.

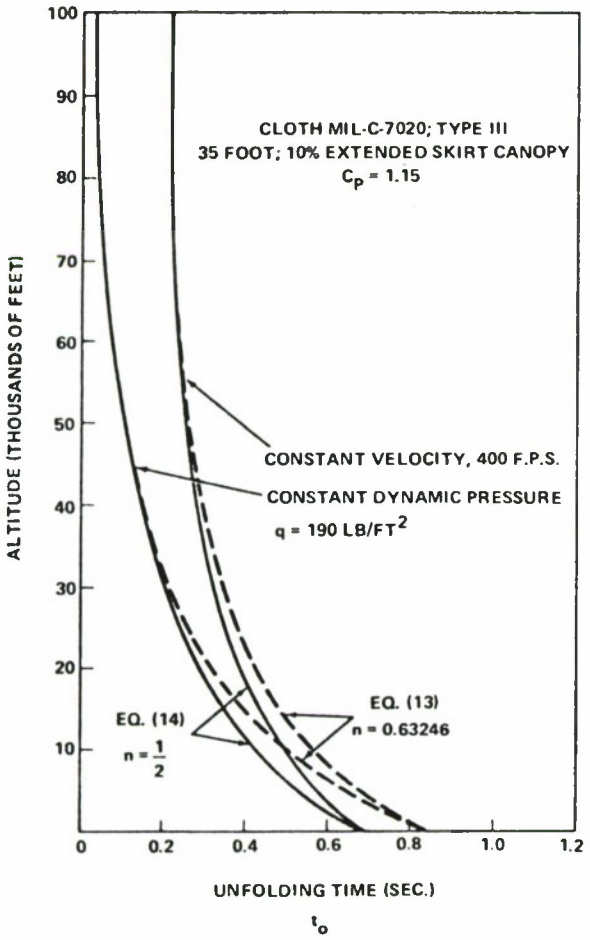

FIG. 12 EFFECT OF ALTITUDE ON THE UNFOLDING TIME "t_o" AT CONSTANT VELOCITY AND CONSTANT DYNAMIC PRESSURE FOR n = 1/2 AND n = 0.63296

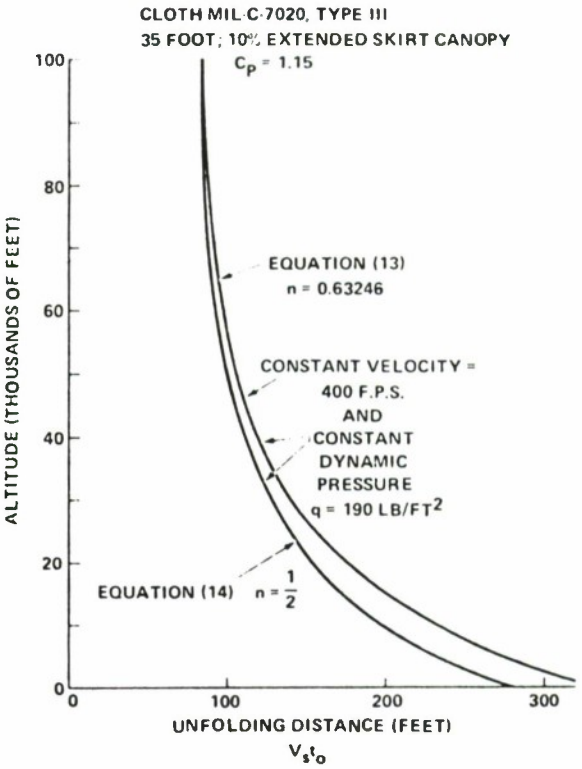

FIG. 13 EFFECT OF ALTITUDE ON THE UNFOLDING DISTANCE AT CONSTANT VELOCITY AND CONSTANT DYNAMIC PRESSURE FOR n = 1/2 AND n = 0.63246.

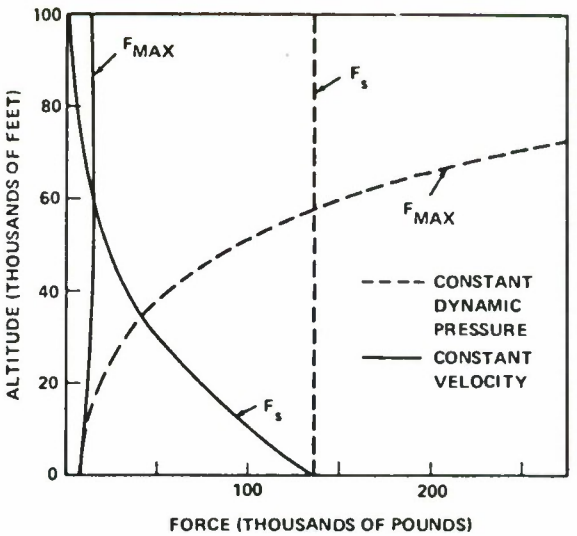

FIG. 14 VARIATION OF STEADY-STATE DRAG, F_s, AND MAXIMUM OPENING SHOCK WITH ALTITUDE FOR CONSTANT VELOCITY AND CONSTANT DYNAMIC PRESSURE

Case A - When the initial projected area is known

$$\frac{A_i}{A_c} = \left(\frac{t_i}{t_o}\right)^3$$

$$t_i = \left(\frac{A_i}{A_c}\right)^{1/3} t_{o_{calculated}}$$

$$t_{o_{corrected}} = \left[1 - \left(\frac{A_i}{A_c}\right)^{1/3}\right] t_{o_{calculated}} \qquad (15)$$

Case B - When the initial drag area is known

$$\frac{C_D S_i}{C_D S_o} = \left(\frac{t_i}{t_o}\right)^6$$

$$t_i = \left(\frac{C_D S_i}{C_D S_o}\right)^{1/6} t_{o_{calculated}}$$

$$t_{o_{corrected}} = \left[1 - \left(\frac{C_D S_i}{C_D S_o}\right)^{1/6}\right] t_{o_{calculated}} \qquad (16)$$

The mass ratio should now be adjusted for the corrected t_o before velocity and force profiles are determined.

VI. Opening-Shock Force, Velocity Ratio, and Inflation Time During the Elastic Phase of Parachute Inflation

The mass ratio, M, is an important parameter in parachute analysis. For values of $M << 4/21$, the maximum opening-shock force occurs early in the inflation process, and the elastic properties of the canopy are not significant. As the mass ratio approaches $M = 4/21$, the magnitude of the opening-shock force increases, and the time of occurrence happens later in the deployment sequence. For mass ratios $M > 4/21$, the maximum shock force will occur after the reference time, t_o. Parachutes designed for high mass ratio operation must provide a structure of sufficient constructed strength, F_c, so that the actual elongation of the canopy under load is less than the maximum extensibility, ϵ_{max}, of the materials.

Development of the analysis in the elastic phase of inflation is similar to the technique used in the unfolding phase. Newton's second law of motion is used, together with the drag area ratio signature and mass ratio

$$\frac{C_D S}{C_D S_o} = \left(\frac{t}{t_o}\right)^6$$

which is still valid, as shown in Figure 7

$$\frac{1}{Mt_o}\int_{t_o}^{t}\left(\frac{t}{t_o}\right)^6 dt = V_s\int_{V_o}^{V}\frac{-dV}{V^2}$$

Integrating and solving for $\frac{V}{V_s}$

$$\frac{V}{V_s} = \frac{1}{\frac{V_s}{V_o} + \frac{1}{7M}\left[\left(\frac{t}{t_o}\right)^7 - 1\right]} \qquad (17)$$

where $\frac{V_o}{V_s}$ is the velocity ratio of the unfolding process at time $t = t_o$.

$$\frac{V_o}{V_s} = \frac{1}{1 + \frac{1}{M}\left[\frac{(1-\eta)^2}{7} + \frac{\eta(1-\eta)}{2} + \eta^2\right]} \qquad (18)$$

The instantaneous shock factor in the elastic phase becomes

$$x_i = \frac{C_D S}{C_D S_o}\left(\frac{V}{V_s}\right)^2$$

$$x_i = \frac{\left(\frac{t}{t_o}\right)^6}{\left[\frac{V_s}{V_o} + \frac{1}{7M}\left[\left(\frac{t}{t_o}\right)^7 - 1\right]\right]^2} \qquad (19)$$

The end point of the inflation process depends upon the applied loads, elasticity of the canopy, and the constructed strength of the parachute. A linear load elongation

relationship is utilized to determine the maximum drag area.

$$\frac{\epsilon}{F} = \frac{\epsilon_{max}}{F_c}$$

$$\epsilon = \frac{F\ \epsilon_{max}}{F_c} \qquad (20)$$

The force, F, is initially the instantaneous force at the end of the unfolding process

$$F = X_o F_s \qquad (21)$$

where X_o is the shock factor of the unfolding phase at $t = t_o$

$$X_o = \frac{1}{\left[1 + \frac{1}{M}\left[\frac{(1-\eta)^2}{7} + \frac{\eta(1-\eta)}{2} + \eta^2\right]\right]^2} \qquad (22)$$

Since the inflated shape is defined, the drag coefficient is considered to be constant, and the instantaneous force is proportional to the dynamic pressure and projected area. The maximum projected area would be developed if the dynamic pressure remained constant during the elastic phase. Under very high mass ratios, this is nearly the case over this very brief time period; but as the mass ratio decreases, the velocity decay has a more significant effect. The simplest approach for all mass ratios is to determine the maximum drag area of the canopy as if elastic inflation had occurred at constant dynamic pressure. Then utilizing the time ratio determined as an end point, intermediate shock factors can be calculated from equation (19) and maximum force assessed.

The initial force, $X_o F_s$, causes the canopy to increase in projected area. The new projected area in turn increases the total force on the canopy which produces a secondary projected area increase. The resulting series of events are resisted by the parachute materials. The parachute must, therefore, be constructed of sufficient strength to prevent the elongation of the materials from exceeding the maximum elongation.

$$\epsilon_o = \frac{X_o F_s}{F_c}\ \epsilon_{max} \qquad (23)$$

The next force in the series at constant q

$$F_1 = X_o F_s \frac{A_1}{A_c}$$

where

$$\frac{A_1}{A_c} = (1 + \epsilon_o)^2$$

Subsequent elongations in the system can be shown to be

$$\epsilon_1 = \epsilon_o\ (1 + \epsilon_o)^2$$

$$\epsilon_2 = \epsilon_o\ (1 + \epsilon_o\ (1 + \epsilon_o)^2)^2$$

The required canopy constructed strength can be determined for a given set of deployment conditions. The limiting value of the series (ϵ_ℓ) determines the end point time ratio.

$$\left(\frac{t_f}{t_o}\right)^6 = \frac{C_D S_{max}}{C_D S_o} = (1 + \epsilon_\ell)^2$$

$$\left(\frac{t_f}{t_o}\right) = \left(\frac{C_D S_{max}}{C_D S_o}\right)^{1/6} = (1 + \epsilon_\ell)^{1/3} \qquad (24)$$

Figure 15 illustrates the maximum drag area ratio as a function of ϵ_o.

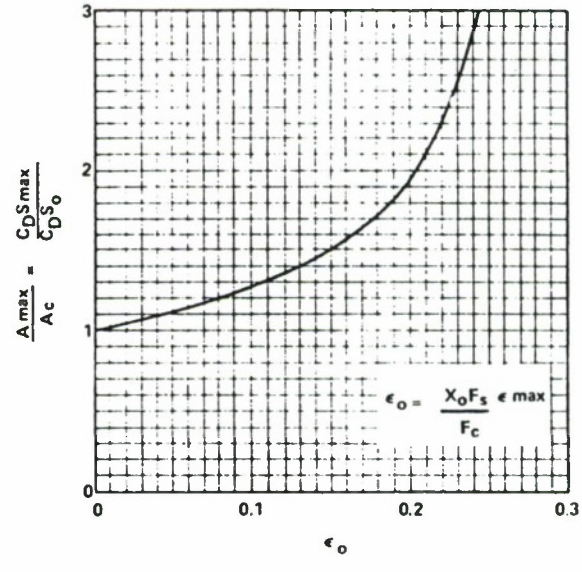

FIG. 15 MAXIMUM DRAG AREA RATIO VS. INITIAL ELONGATION

VII. Application of Cloth Permeability to the Calculation of the Inflation Time of Solid Cloth Parachutes

The mass outflow through the pressurized region of an inflating solid cloth parachute at any instant is dependent upon the canopy area which is subjected to airflow and the rate of airflow through that area. The variation of pressurized area as a function of reference time, t_o, was earlier assumed to be proportional to the instantaneous drag area ratio, leaving the rate-of-airflow problem to solve. The permeability parameter of cloth was a natural choice for determining the rate of airflow through the cloth as a function of pressure differential across the cloth. Heretofore, these data have been more of a qualitative, rather than quantitative, value. A new method of analysis was developed wherein a generalized curve of the form $P = k(\Delta P)^n$ was fitted to cloth permeability data for a number of different cloths and gives surprisingly good agreement over the pressure differential range of available data. The pressure differential was then related to the trajectory conditions to give a generalized expression which can be used in the finite mass ratio range, as well as the infinite mass case. The permeability properties were transformed into a mass flow ratio, M', which shows agreement with the effective porosity concept.

Measured and calculated permeability pressure data for several standard cloths are illustrated in Figure 16. This method has been applied to various types of cloth between the extremes of a highly permeable 3-momme silk to a relatively impervious parachute pack container cloth with reasonably good results, see Figure 17.

The canopy pressure coefficient, C_p, is defined as the ratio of the pressure differential across the cloth to the dynamic pressure of the free stream.

$$C_p = \frac{\Delta P}{q} = \frac{P(\text{internal}) - P(\text{external})}{1/2\ \rho V^2} \qquad (25)$$

where V is based on equation (7).

The permeability expression, $P = k(\Delta P)^n$ becomes

$$P = k\left(C_p \frac{\rho V^2}{2}\right)^n \qquad (26)$$

Although some progress has been made by Melzig and others on the measurement of the variation of the pressure coefficient on an actual inflating canopy, this dimension and its variation with time are still dark areas at the time of this writing. At the present time, a constant average value of pressure coefficient is used in these calculations. Figure 18 presents the effect of pressure coefficient and altitude on the unfolding time for constant deployment conditions.

It is well known that the inflation time of solid cloth parachutes decreases as the operational altitude increases. This effect can be explained by considering the ratio of the mass outflow through a unit cloth area to the mass inflow through a unit mouth area.

$$M' = \text{mass flow ratio} = \frac{\text{mass outflow}}{\text{mass inflow}}$$

where

$$\text{mass outflow} = P_{\rho}\ \frac{\text{slugs}}{\text{ft}^2\text{-sec}}\ (\text{per ft}^2 \text{ cloth area})$$

and

$$\text{mass inflow} = V_{\rho}\ \frac{\text{slugs}}{\text{ft}^2\text{-sec}}\ (\text{per ft}^2 \text{ inflow area})$$

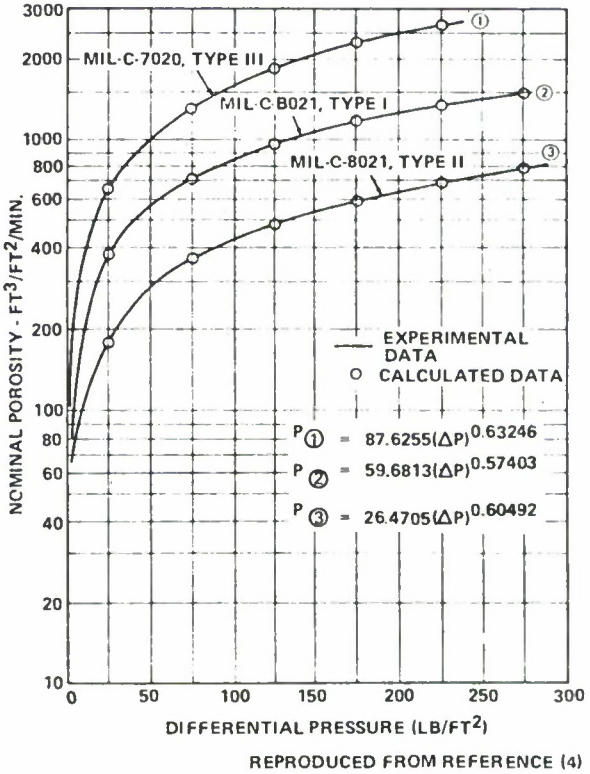

REPRODUCED FROM REFERENCE (4)

FIG. 16 NOMINAL POROSITY OF PARACHUTE MATERIAL VS DIFFERENTIAL PRESSURE.

Therefore, the mass flow ratio becomes

$$M' = \frac{P\rho}{V\rho} = \frac{P}{V}$$

$$M' = k\left(\frac{C_p\rho}{2}\right)^n V^{(2n-1)} \qquad (27)$$

Effective porosity, C, is defined as the ratio of the velocity through the cloth, u, to a fictitious theoretical velocity, v, which will produce the particular $\Delta P = 1/2\rho v^2$.

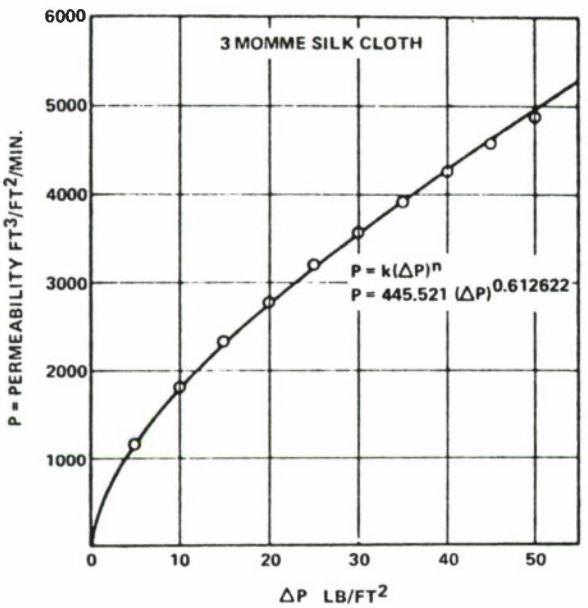

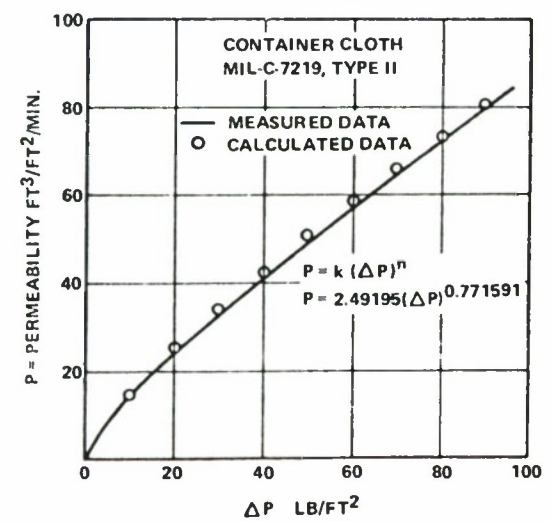

FIG. 17 COMPARISON OF MEASURED AND CALCULATED PERMEABILITY FOR RELATIVELY PERMEABLE AND IMPERMEABLE CLOTHS

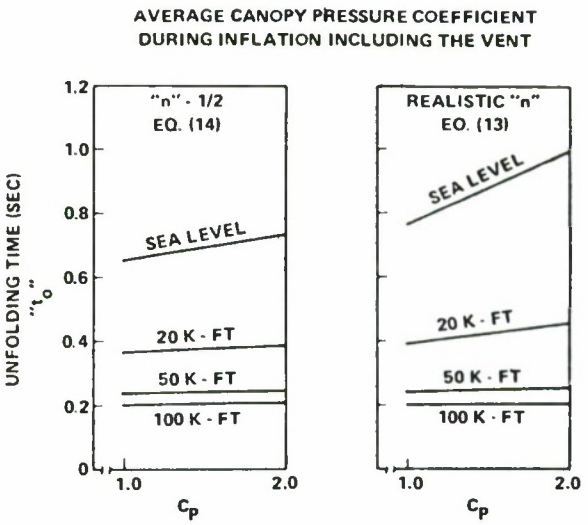

FIG. 18 EFFECT OF PRESSURE COEFFICIENT AND ALTITUDE ON THE UNFOLDING TIME.

$$\text{effective porosity, } C = \frac{u}{v} \qquad (28)$$

Comparison of the mass flow ratio and previously published effective porosity data is shown in Figure 19. The effects of altitude and velocity on the mass flow ratio are presented in Figures 20, and 21 for constant velocity and constant altitude. The decrease of cloth permeability with altitude is evident.

The permeability constants "k" and "n" can be determined from the permeability pressure differential data as obtained from an instrument such as a Frazier Permeameter. Two data points, "A" and

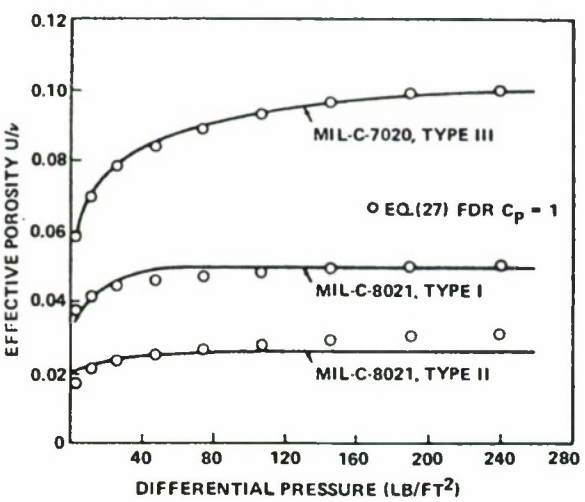

REPRODUCED FROM REFERENCE (4)

FIG. 19 THE EFFECTIVE POROSITY OF PARACHUTE MATERIALS VS. DIFFERENTIAL PRESSURE

"B," are selected in such a manner that point "A" is in a low-pressure zone below the knee of the curve, and point "B" is located in the upper end of the high-pressure zone, as shown in Figure 22.

The two standard measurements of 1/2 inch of water and 20 inches of water appear to be good data points if both are

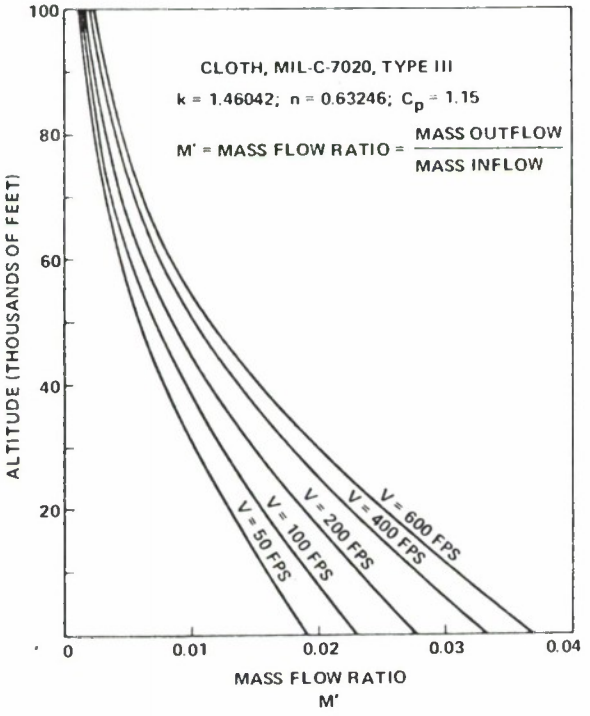

FIG. 20 EFFECT OF ALTITUDE ON MASS FLOW RATIO AT CONSTANT VELOCITY

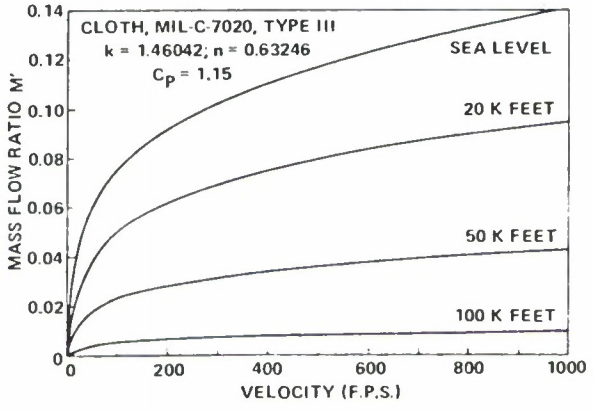

FIG. 21 EFFECT OF VELOCITY ON MASS FLOW RATIO AT CONSTANT DENSITY

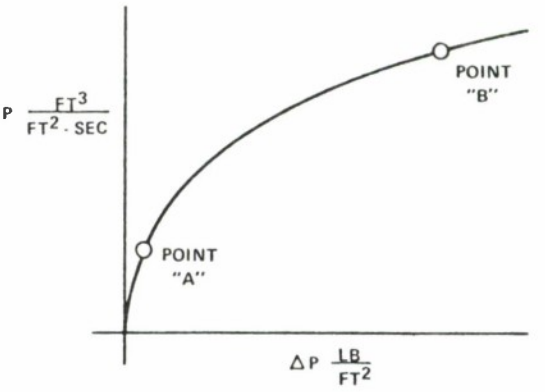

FIG. 22 LOCATION OF DATA POINTS FOR DETERMINATION OF "k" AND "n"

available on the same sample. Substituting the data from points "A" and "B" into $P = k(\Delta P)^n$:

$$n = \frac{\ell n\left(\frac{P_B}{P_A}\right)}{\ell n\left(\frac{\Delta P_B}{\Delta P_A}\right)} \qquad (29)$$

$$k = \frac{P_A}{(\Delta P_A)^n} = \frac{P_B}{(\Delta P_B)^n} \qquad (30)$$

VIII. Determination of the Parachute Included Volume and Associated Air Mass

Before the reference time, t_o, and inflation time, t_f, can be calculated, the volume of atmosphere, V_o, which is to be collected during the inflation process must be accurately known. This requirement dictates that a realistic inflated canopy shape and associated volume of atmosphere be determined. Figure 23 was reproduced from reference (5). The technique of using lampblack coated plates to determine the airflow patterns around metal models of inflated canopy shapes was used by the investigator of reference (5) to study the stability characteristics of contemporary parachutes, i.e., 1943. A by-product of this study is that it is clearly shown that the volume of air within the canopy bulges out of the canopy mouth (indicated by arrows) and extends ahead of the canopy hem. This volume must be collected during the inflation process. Another neglected, but significant, source of canopy volume exists in the billowed portion of the gore panels.

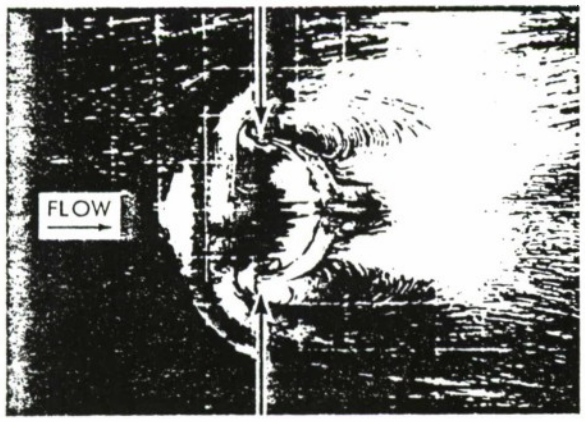

HEMISPHERE

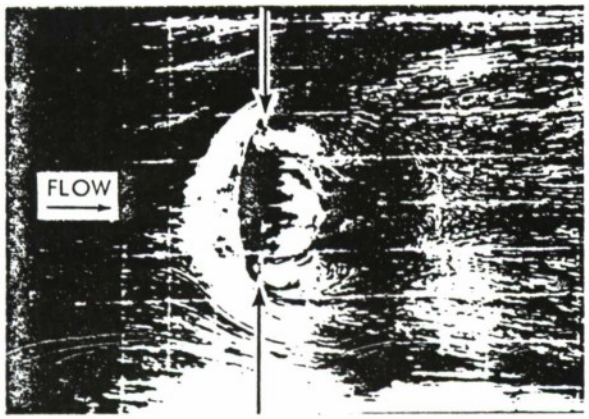

VENT PARACHUTE

REPRODUCED FROM REFERENCE (5)

FIG. 23 AIRFLOW PATTERNS SHOWING AIR VOLUME AHEAD OF CANOPY HEM

The steady-state canopy shape has been observed in wind-tunnel and field tests to be elliptical in profile. Studies of the inflated shape and included volume of several parachute types (flat circular, 10 percent extended skirt, elliptical, hemispherical, ring slot, ribbon, and cross) are documented in references (6) and (7). These studies demonstrated that the steady-state profile shape of inflated canopies of the various types can be approximated to be two ellipses of common major diameter, $2\bar{a}$, and dissimilar minor diameters, b and b', as shown in Figure 24. It was also shown that the volume of the ellipsoid of revolution formed by revolving the profile shape about the canopy axis was a good approximation of the volume of atmosphere to be collected during canopy inflation and included the air volume extended ahead of the parachute skirt hem together with the billowed gore volume.

$$\underline{V}_o = \frac{2}{3}\ \pi\bar{a}^3 \left[\frac{b}{\bar{a}} + \frac{b'}{\bar{a}}\right] \qquad (31)$$

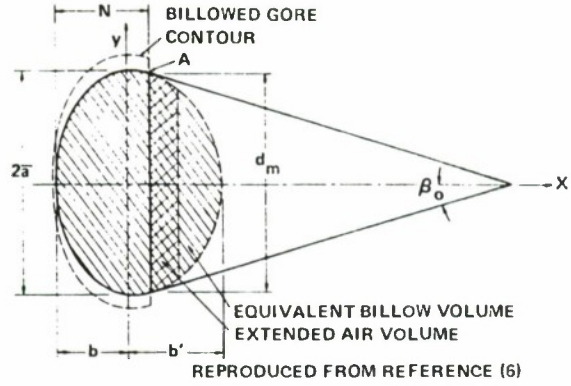

REPRODUCED FROM REFERENCE (6)

FIG. 24 PARACHUTE CROSS SECTION NOMENCLATURE

Tables I and II are summaries of test results reproduced from references (6) and (7), respectively, for the convenience of the reader.

IX. References

1. "A Method to Reduce Parachute Inflation Time with a Minor Increase in Opening Force," WADD Report TR 60-761
2. Berndt, R. J., and DeWesse, J. H., "Filling Time Prediction Approach for Solid Cloth Type Parachute Canopies," AIAA Aerodynamic Deceleration Systems Conference, Houston, Texas, 7-9 Sep 1966
3. "Theoretical Parachute Investigations," Progress Report No. 4, Project No. 5, WADC Contract AF33 (616)-3955, University of Minnesota
4. "Performance of and Design Criteria for Deployable Aerodynamic Decelerators," TR ASK-TR-61-579, AFFDL, AIRFORCESYSCOM, Dec 1963
5. "Investigation of Stability of Parachutes and Development of Stable Parachutes from Fabric of Normal Porosity," Count Zeppelin Research Institute Report No. 300, 23 Mar 1943
6. Ludtke, W. P., "A New Approach to the Determination of the Steady-State Inflated Shape and Included Volume of Several Parachute Types," NOLTR 69-159, 11 Sep 1969
7. Ludtke, W. P., "A New Approach to the Determination of the Steady-State Inflated Shape and Included Volume of Several Parachute Types in 24-Gore and 30-Gore Configurations," NOLTR 70-178, 3 Sep 1970

TABLE I SUMMARY OF PARACHUTE SHAPE TEST RESULTS FOR 12-GORE AMD 16-GORE CONFIGURATIONS

Parachute Type	No. of Gores	Suspension Line Length inches	Velocity mph	Velocity fps	Scale Factor, K $\frac{2\bar{a}}{D_o}$	$\frac{2\bar{a}}{D_F}$	$\frac{2\bar{a}}{D_R}$	$\frac{2\bar{a}}{L}$	$\frac{N}{\bar{a}}$	Axes Ratio $\frac{b}{\bar{a}}$	$\frac{b'}{\bar{a}}$	$\frac{b}{\bar{a}}+\frac{b'}{\bar{a}}$	Volume in^3 V_H	V_C	V_o	$\frac{V_o}{V_H}$
Flat Circular	12	34	50	73	.645	.650			.856	.6115	.8817	1.4932	4476	4481	6980	1.56
	16	34	50	73	.663	.669			.820	.5558	.9039	1.4597	4450	4100	7325	1.65
10% Extended Skirt	12	34	100	147	.663	.652			.881	.6424	.8860	1.5284	3928	4400	6783	1.73
	16	34	17	25	.654	.640			.785	.5580	.8502	1.4082	4051	3920	6197	1.53
Elliptical	12	34	75	110			.916		.812	.5626	.9657	1.5283		3322	5405	
	16	34	17	25			.875		.800	.6169	8163	1.4332		2726	4405	
Hemispherical	12	34	125	183			.996		1.254	1.0005	.9080	1.9085		6224	8666	
	16	34	75	110			.994		1.185	.9129	.9380	1.8509		5921	8370	
Ringslot 16% Geometric Porosity	12	34	25	37	.607	.654			.853	.6566	.8735	1.530	3800	3650	5903	1.55
	12	34	100	147	.616	.663			.922	.6566	.8735	1.530	3800	4198	6166	1.62
	12	34	200	293	.637	.686			.918	.6566	.8735	1.530	3800	4624	6826	1.90
	16	34	25	37	.611	.658			.827	.6004	.8890	1.4894	3800	3763	5685	1.50
	16	34	100	147	.617	.664			.864	.6004	.8890	1.4894	3800	3985	6030	1.59
	16	34	200	293	.645	.695			.844	.6004	.8890	1.4894	3800	4430	6897	1.82
Ribbon 24% Geometric Porosity	12	34	25	37	.586	.632			.859	.6558	.8768	1.5326	3800	3323	5335	1.40
	12	34	100	147	.615	.663			.837	.6558	.8768	1.5326	3800	3714	6163	1.62
	12	34	200	293	.632	.681			.877	.6558	.8768	1.5326	3800	4280	6683	1.76
	16	34	25	37	.603	.650			.797	.5570	.8578	1.4148	3800	3438	5358	1.41
	16	34	100	147	.626	.674			.791	.5570	.8578	1.4148	3800	3804	5983	1.57
	16	34	200	293	.648	.698			.781	.5570	.8578	1.4148	3800	4164	6656	1.75
Cross Chute w/L = .264		34	25	37	.710			.543	1.242	.8867	1.2776	2.1643	1928	3768	5798	3.01
		34	100	147	.707			.540	1.270	.8867	1.2776	2.1643	1928	3810	5712	2.96
		34	200	293	.716			.547	1.285	.8867	1.2776	2.1643	1928	4212	5925	3.07
		47	25	37	.759			.580	1.113	.8494	1.2512	2.1006	1928	4052	6868	3.56
		47	100	147	.729			.557	1.205	.8494	1.2512	2.1006	1928	3973	5958	3.09
		47	200	293	.775			.592	1.110	.8494	1.2512	2.1006	1928	4292	7303	3.79

REPRODUCED FROM REFERENCE (6)

TABLE II SUMMARY OF PARACHUTE SHAPE TEST RESULTS FOR 24-GORE AND 30-GORE CONFIGURATIONS

Parachute Type	No. of Gores	Suspension Line Length inches	Velocity mph	Velocity fps	Scale Factor, K $\frac{2\bar{a}}{D_o}$	$\frac{2\bar{a}}{D_F}$	$\frac{N}{\bar{a}}$	Axes Ratio $\frac{b}{\bar{a}}$	$\frac{b'}{\bar{a}}$	$\frac{b}{\bar{a}}+\frac{b'}{\bar{a}}$	Volume in^3 V_H	V_c	V_o	$\frac{V_o}{V_H}$
Flat Circulars	24	34	50	73	.677	.679	.795	.5758	.8126	1.3884	4362	4695	7273	1.67
	30	34	17	25	.668	.669	.827	.6214	.7806	1.4020	4342	4626	7027	1.62
10% Extended* Skirt	24	34	100	147	.665	.648	.834	.5949	.8771	1.4720	4138	4446	6930	1.67
	30	34	17	25	.650	.633	.825	.6255	.7962	1.4127	4172	4076	6265	1.50
Ring Slot 16% Geometrically Porous	24	34	25	37	.663	.665	.824	.5800	.9053	1.4853	3591	3878	6031	1.68
	24	34	100	147	.680	.682	.819	.5800	.9053	1.4853	3591	4079	6510	1.81
	24	34	200	293	.694	.696	.809	.5800	.9053	1.4853	3591	4270	6924	1.93
	30	34	25	37	.677	.678	.788	.5800	.9053	1.4853	3582	3826	6404	1.79
	30	34	100	147	.684	.685	.802	.5800	.9053	1.4853	3582	4023	6588	1.84
	30	34	200	293	.698	.699	.800	.5800	.9053	1.4853	3582	4260	7012	1.96
Ribbon 24% Geometrically Porous	24	34	25	37	.671	.673	.770	.5980	.8187	1.4167	3591	3591	5968	1.66
	24	34	100	147	.676	.678	.813	.5980	.8187	1.4167	3591	3927	6097	1.70
	24	34	200	293	.687	.689	.804	.5980	.8187	1.4167	3591	4061	6389	1.78
	30	34	25	37	.655	.657	.782	.6021	.8463	1.4484	3582	3396	5666	1.58
	30	34	100	147	.669	.670	.784	.6021	.8463	1.4484	3582	3622	6022	1.68
	30	34	200	293	.677	.679	.823	.6021	.8463	1.4484	3582	4002	6256	1.75

*Since this parachute was "breathing" during the test, several photographs were taken at each speed. The data were reduced from the photograph which most reasonably appeared to represent the equilibruim state.

REPRODUCED FROM REFERENCE (7)

X. List of Symbols

A_c - Steady-state projected area of the inflated parachute, ft^2

A_M - Instantaneous canopy mouth area, ft^2

A_{Mo} - Steady-state inflated mouth area, ft^2

a - Acceleration, ft/sec^2

$2\bar{a}$ - Maximum inflated parachute diameter of gore mainseam, ft

b - Minor axis of the ellipse bounded by the major axis ($2\bar{a}$) and the vent of the canopy, ft

b' - Minor axis of the ellipse which includes the skirt hem of the canopy, ft

C - Effective porosity

C_D - Parachute coefficient of drag

C_p - Parachute pressure coefficient, relates internal and external pressure (ΔP) on canopy surface to the dynamic pressure of the free stream

D_o - Nominal diameter of the aerodynamic decelerator = $\sqrt{4S_o/\pi}$, ft

F - Instantaneous force, lbs

F_s - Steady-state drag force that would be produced by a fully open parachute at velocity V_s, lbs

F_c - Constructed strength of the parachute, lbs

F_{max} - Maximum opening-shock force, lbs

g - Gravitational acceleration, ft/sec^2

k - Permeability constant of canopy cloth

m - Mass, slugs

M - Mass ratio - ratio of the mass of the retarded hardware (including parachute) to a mass of atmosphere contained in a right circular cylinder of length ($V_s t_o$), face area ($C_D S_o$), and density (ρ)

M' - Mass flow ratio - ratio of atmosphere flowing through a unit cloth area to the atmosphere flowing through a unit inlet area at arbitrary pressure

n - Permeability constant of canopy cloth

P - Cloth permeability - rate of airflow through a cloth at an arbitrary differential pressure, $ft^3/ft^2/sec$

q - Dynamic pressure, lb/ft^2

$S = A_s$ - Instantaneous inflated canopy surface area, ft^2

$S_o = A_{so}$ - Canopy surface area, ft^2

t - Instantaneous time, sec

t_o - Reference time when the parachute has reached the design drag area for the first time, sec

t_f - Canopy inflation time when the inflated canopy has reached its maximum physical size, sec

u - Air velocity through cloth in effective porosity, ft/sec

v - Fictitious theoretical velocity used in effective porosity, ft/sec

V - Instantaneous system velocity, ft/sec

V_o - System velocity at the time $t = t_o$, ft/sec

V_s - System velocity at the end of suspension line stretch, ft/sec

$\underline{V}_o$ - Volume of air which must be collected during the inflation process, ft^3

W - Hardware weight, lb

x_1 - Instantaneous shock factor

X_o - Shock factor at the time $t = t_o$

ρ - Air density, $slugs/ft^3$

η - Ratio of parachute projected mouth area at line stretch to the steady-state projected area

ϵ - Instantaneous elongation

ϵ_{max} - Maximum elongation

ϵ_o - Initial elongation at the beginning of the elastic phase of inflation

S.F. - Parachute safety factor = F_c/F_{max}

Appendix B

A GUIDE FOR THE USE OF APPENDIX A

At first reading, Appendix A may appear to be a complicated system of analysis because of the many formulae presented. Actually, once understood, the technique is straightforward and uncomplicated. The author has attempted to simplify the algebra wherever possible. This appendix presents, in semi-outline form, a guide to the sequence of calculations because the analysis does require use of formulae from the text, not necessarily in the order in which they were presented. Also, the user can be referred to graphs of performance to illustrate effects.

In order to compute t_o, other parameters must be obtained from various sources.

I. Determine System Parameters

1. $C_D S_o$, drag area, ft^2 obtained from design requirement.

2. V_s, fps, velocity of system at suspension line stretch.

3. ρ, slugs/ft^3, air density at deployment altitude.

4. W, lb, system weight (including weight of the parachute) from design requirements.

5. $\underline{V}_o$, ft^3, this volume of air, which is to be collected during inflation, is calculated from the steady-state inflated shape geometry of the particular parachute type. The nomenclature is described in Figure 24,p.A-14. When D_o or D_F is known, $\bar{a}$ can be calculated from data in Table I and Table II, p. A-15, for various parachute types and number of gores. Then the geometric volume $\underline{V}_o$ can be calculated by Equation (31), p. A-14, with appropriate values of $b/\bar{a}$ and $b'/\bar{a}$ from the tables.

6. A_{MO}, ft^2, steady-state canopy mouth area

$$A_{MO} = \pi \bar{a}^2 \left[1 - \left(\frac{N/\bar{a} - b/\bar{a}}{b'/\bar{a}} \right)^2 \right] \qquad \text{(B-1)}$$

where $N/\bar{a}$, $b/\bar{a}$, and $b'/\bar{a}$ are available from Tables I and II for the particular type of parachute and number of gores.

7. A_{so}, ft^2, canopy surface area = $\frac{\pi}{4}D_o^2$

8. C_p, pressure coefficient, see Figure 18, p. A-12. A constant $C_p = 1.7$ for all altitudes seems to yield acceptable results.

9. Constants k and n are derived from measurements of the air flow through the cloth. Only k is needed for Equation (14), but n is also required for Equation (13). These parameters can be determined for any cloth using the technique described beginning on p. A-12. The two-point method is adequate if the ΔP across the cloth is in the range of ΔP for actual operation. Check-points of cloth permeability can be measured and compared to calculated values to verify agreement. If the data are to be extrapolated to operational ΔP's greater than measured, a better method of determining k and n from the test data would be a least squares fit through many data points. This way errors due to reading either of the two points are minimized.

II. Step 1

Calculate the reference time t_o by use of Equations (13) or (14), p. A-7. If the deployment altitude is 50,000 feet or higher, Equation (14) is preferred due to its simplicity. For altitudes from sea level to 50,000 feet, Equation (13) is preferred. Figure 12, p. A-8, shows the effect of altitude on t_o and can be taken as a guide for the user to decide whether to use Equation (13) or (14). One should keep in mind that the opening shock force can be a strong function of inflation time, so be as realistic as possible. If Equation (13) is elected, the method in use at the NSWC/WO is to program Equation (13) to compute the parachute volume, $\underline{V}_o$, for an assumed value of t_o. Equation (14), because of its simplicity, can be used for a first estimate of t_o at all altitudes. The computed canopy volume is then compared to the canopy volume calculated from the geometry of the parachute as per Equation (31), p. A-14. If the volume computed from the mass flow is within the volume computed from the geometry within plus or minus a specified delta volume, the time t_o is printed out. If not within the specified limits, t_o is adjusted, and a new volume calculated. For a 35-foot D_o, T-10 type canopy, I use plus or minus 10 cubic feet in the volume comparison. The limit would be reduced for a parachute of smaller D_o.

If $\underline{V}_o$ calculated = $\underline{V}_o$ geometry $\pm$ 10, then print answer.

If $\underline{V}_o$ calculated $\neq$ $\underline{V}_o$ geometry $\pm$ 10, then correct t_o as follows:

$$t_o = t_o \frac{\underline{V}_{o\ \text{geometry}}}{\underline{V}_{o\ \text{calculated}}} \qquad \text{(B-2)}$$

The new value of t_o is substituted in the "do loop" and the volume recomputed. This calculation continues until the required volume is within the specified limits.

III. Calculate t_o corrected for initial area. The t_o of Section II assumes that the parachute inflated from a zero initial area. If this is a reasonable assumption for the particular system under study, then the mass ratio can be determined from Equation (6), p. A-4. For $\eta = 0$ if the value of $M \leq 0.19$, then a finite state of deployment exists, and the time ratio of occurrence and the maximum shock factor can be determined from Equations (9) and (10), respectively, on p. A-5. If $\eta \neq 0$, then the limiting mass ratio for finite operations will rise slightly as described in Appendix C. Figures C-1 and C-2 illustrate the effects of initial area on limiting mass ratios and shock factors respectively. If the mass ratio is greater than the limiting mass ratio (M_L), then the maximum shock force occurs at a time greater than t_o and the elasticity of the materials must be considered (see Section VI).

If $\eta \neq 0$, then the reference time, t_o, will be reduced, and the mass ratio will rise due to partial inflation at the line stretch. Figures 9 and 10, p. A-6, illustrate the effects of initial area on the velocities and shock factor during the "unfolding" inflation. Equation (15), p. A-9, can be used to correct t_o calculated for the cases where $\eta = Ai/Ac$. If the initial value of drag area is known, Equation (16), p. A-9, can be used to correct t_o and rechecked for limiting mass ratios versus η in Appendix C.

IV. Opening shock calculations in the elastic phase of inflation. It has been considered that from time $t = 0$ to $t = t_o$ the parachute has been inelastic. At the time $t = t_o$ the applied aerodynamic load causes the materials to stretch and the parachute canopy increases in size. The increased size results in an increase in load, which causes further growth, etc. This sequence of events continues until the applied forces have been balanced by the strength of materials. The designer must insure that the constructed strength of the materials is sufficient to resist the applied loads for the material elongation expected. Use of materials of low elongation should result in lower opening shock forces as $C_D S_{max}$ is reduced.

When the mass ratio of the system is greater than the limiting mass ratio, the elasticity of the materials and material strength determine the maximum opening shock force. The maximum elongation ε_{max} and the ultimate strength of the materials are known from tests or specifications. The technique begins on p. A-9.

At the time $t = t_o$, calculate the following quantities for the particular values of M and η.

a. V_o/V_s from Equation (18), p. A-9.

b. X_o from Equation (22), p. A-10.

c. ε_o from Equation (23), p. A-10.

d. Determine $C_D S_{max}/C_D S_o$ from Figure 15, p. A-10.

e. Calculate the inflation time ratio t_f/t_o from Equation (24), p. A-10.

f. Calculate the maximum shock factor from Equation (19), p. A-9.

g. Calculate the opening shock force $F_{max.} = X_1 F_S$ where

$$F_S = \frac{1}{2}\rho V_S^2 C_D S_o$$

h. Calculate filling time, t_f(sec)

$$t_f = t_o \left(\frac{t_f}{t_o}\right)$$

V. In order to simplify the required effort, the work sheets of Table B-1 are included on pages B-5 through B-9 to aid the engineer in systematizing the analysis. The work sheets should be reproduced to provide additional copies.

Table B-1. Opening Shock Force

CALCULATION WORK SHEETS	SYMBOL	VALUE	DIMENSION
1. Parachute type -			
2. System parameters			
a. System weight, W (lb)	W		lb.
b. Gravity, g (ft/sec^2)	g		ft/sec^2
c. Deployment altitude (ft)			ft.
d. Deployment air density, ρ ($slugs/ft^3$)	ρ		$slugs/ft^3$
e. Velocity at line stretch, V_s (fps)	V_s		fps.
f. Steady state canopy data			
(1) Diameter, D_o (ft)	D_o		ft.
(2) Inflated diameter, $2\bar{a}$ (ft); $\frac{2\bar{a}}{D_o} = *$	$2\bar{a}$		ft.
(3) Surface area, S_o (ft^2); $\frac{\pi}{4} D_o^2$	$A_{so} = S_o$		$ft.^2$
(4) Drag area, $C_D S_o$ (ft^2); $C_D \times S_o$	$C_D S_o$		$ft.^2$
(5) Mouth area, A_{MO}^* (ft^2)			
$A_{MO} = \pi \bar{a}^2 \left[1 - \left(\frac{N/\bar{a} - b/\bar{a}}{b'/\bar{a}}\right)^2\right]$	A_{MO}		$ft.^2$
(6) Volume, V_o^* (ft^3)			
$V_o = \frac{2}{3} \pi \bar{a}^3 \left[\frac{b}{\bar{a}} + \frac{b'}{\bar{a}}\right]$	V_o		$ft.^3$
g. Cloth data			
(1) k } Calculate using technique beginning on	k		—
(2) n } p. A-12. Note: Permeability is usually measured as $ft^3/ft^2/min$. For these calculations permeability must be expressed as $ft^3/ft^2/sec$	n		—

* Data for these calculations are listed in Tables 1 and 2, p. A-15.

Table B-1. Opening Shock Force (cont'd)

	SYMBOL	VALUE	DIMENSION
(3) ε_{max}; determine maximum elongations from pull test data of joints, seams, lines, etc. Use minimum ε_{max} determined from tests.			
(4) Cp; pressure coefficient	C_p		—
h. Steady state drag, F_s (lb), $F_s = \frac{1}{2}\rho V_s^2 C_D S_o$	F_s		lb.
i. Parachute constructed strength, F_c (lb); determined from data on efficiency of seams, joints, lines. Constructed strength is the minimum load required to fail a member times the number of members.	F_c		lb.
3. Force calculations			
a. Calculate t_o for $\eta = 0$; eq. 14, p. A-7. $t_o = \frac{14W}{\rho g V_s C_D S_o}\left[\epsilon^{\frac{\rho g V_o}{2W}\left[\frac{C_D S_o}{A_{MO} - A_{SO}\, k\left(\frac{C_p \rho}{2}\right)^{\frac{1}{2}}}\right]} - 1\right]$	t_o		sec.
Check Figure 13, p. A-8, for advisability of using eq. 13, p. A-7.			
b. If $\eta = 0$, proceed with steps c through e. If $\eta \neq 0$, go to step f.			
c. Mass ratio, M; eq. 6, p. A-4 $M = \frac{2W}{\rho g V_s t_o C_D S_o}$	M		—
d. If $M \leq 4/21$ for $\eta = 0$, then finite mass deployment is indicated.			
(1) Time ratio at $x_{i\ max}$; eq. 9, p. A-5 $\frac{t}{t_o @ x_{i_{max}}} = \left(\frac{21M}{4}\right)^{\frac{1}{7}}$	$\frac{t}{t_o @ x_{i_{max}}}$		—
(2) Max shock factor, x_i; eq., 10, p. A-5 $x_{i_{max}} = \frac{16}{49}\left(\frac{21M}{4}\right)^{\frac{6}{7}}$	$x_{i_{max}}$		—

Table B-1. Opening Shock Force (Cont'd)

	SYMBOL	VALUE	DIMENSION
(3) Max shock force, F_{max} (lb) $F_{max.} = \chi_{i\ max.} F_S$	F_{max}		lb.
e. If M > 4/21; then intermediate mass or infinite mass deployment is indicated and the elasticity of materials is involved. Calculate the trajectory conditions at time t = t_o.			
(1) Velocity ratio @ t = t_o for η = 0 $\frac{V_o}{V_S} = \frac{1}{1 + \frac{1}{7M}}$	$\frac{V}{V_o}$		–
(2) Shock factor X_o @ t = t_o for η = 0 $X_o = \frac{1}{\left[1+\frac{1}{7M}\right]^2} = \left(\frac{V_o}{V_S}\right)^2$	X_o		–
(3) Initial elongation, ε_o; eq. 23, p. A-10 $\epsilon_o = \frac{X_o F_S}{F_c} \epsilon_{max}$	ϵ_o		–
(4) Determine $\frac{C_D S_{max}}{C_D S_o}$ from Figure 15, p. A-10	$\frac{C_D S_{max}}{C_D S_o}$		–
(5) Calculate inflation time ratio, $\frac{t_f}{t_o}$; eq. 24, p. A-10 $\frac{t_f}{t_o} = \left(\frac{C_D S_{max}}{C_D S_o}\right)^{\frac{1}{6}}$	$\frac{t_f}{t_o}$		–
(6) Calculate maximum shock factor, $x_{i\ max}$; eq. 19, p. A-9 $\chi_{i_{max}} = \frac{\left(\frac{t_f}{t_o}\right)^6}{\left[\frac{V_S}{V_o} + \frac{1}{7M}\left[\left(\frac{t_f}{t_o}\right)^7 - 1\right]\right]^2}$	$\chi_{i_{max}}$		–
(7) Calculate maximum shock force, F_{max} (lb), $F_{max} = \chi_{i_{max}} F_S$	F_{max}		lb.

Table B-1. Opening Shock Force (cont'd)

	SYMBOL	VALUE	DIMENSION
(8) Inflation time, sec = $t_f = t_o \left(\frac{t_f}{t_o}\right)$	t_f		Sec.
f. If $\eta \neq 0$, correct t_o for initial area effects; eq. 16, p. A-9 $t_o = \left[1 - \left(\frac{C_D S_i}{C_D S_o}\right)^{1/6}\right] t_{o\ calculated}$	t_o		Sec.
g. Mass Ratio, M, eq. 6, p. A-4 $M = \frac{2W}{\rho g V_s t_o C_D S_o}$	M		–
h. Calculate limiting mass ratio, M_L $M_L = \frac{1}{3(1-\eta)} - \left[\frac{9}{14}\eta^2 + \frac{3}{14}\eta + \frac{1}{7}\right]$	M_L		–
If $M \leq M_L$, finite mass deployment is indicated and $x_{i\ max}$ can be determined by eq. 8, p. A-5 by assuming values of t/t_o and plotting the data using the methods of Appendix C.			
i. If $M > M_L$, then intermediate mass or infinite mass deployment is indicated and the elasticity of materials is involved. Calculate the trajectory conditions at time $t = t_o$.			
(1) Velocity ratio @ $t = t_o$ for $\eta \neq 0$; eq. 18, p. A-9 $\frac{V_o}{V_S} = \frac{}{\left[1 + \frac{1}{M}\left[\frac{(1-\eta)^2}{7} + \frac{\eta(1-\eta)}{2} + \eta^2\right]\right.}$	$\frac{V_o}{V_s}$		–
(2) Shock factor X_o @ $t = t_o$ for $\eta \neq 0$; eq. 22, p. A-10 $X_o = \frac{1}{\left[1 + \frac{1}{M}\left[\frac{(1-\eta)^2}{7} + \frac{\eta(1-\eta)}{2} + \eta^2\right]\right]^2} = \left(\frac{V_o}{V_S}\right)^2$	X_o		–
(3) Initial elongation, ε_o; eq. 23, p. A-10 $\epsilon_o = \frac{X_o F_S}{F_c}\ \epsilon_{max}$	ϵ_o		–
(4) Determine $\frac{C_D S_{max}}{C_D S_o}$ from Figure 15, p. A-10	$\frac{C_D S_{max}}{C_D S_o}$		–

Table B-1. Opening Shock Force (Conta

	SYMBOL	VALUE	DIMENSION
(5) Calculate inflation time ratio, $\frac{t_f}{t_o}$; eq. 24, p. A-10 $\frac{t_f}{t_o} = \left(\frac{C_D S_{max}}{C_D S_o}\right)^{\frac{1}{6}}$	$\frac{t_f}{t_o}$		–
(6) Calculate maximum shock factor, $x_{i\ max}$; eq. 19, p. A-9 $\chi_{i_{max}} = \frac{\left(\frac{t_f}{t_o}\right)^6}{\left[\frac{V_S}{V_o} + \frac{1}{7M}\left[\left(\frac{t_f}{t_o}\right)^7 - 1\right]\right]^2}$	$\chi_{i_{max}}$		–
(7) Calculate maximum shock force, F_{max}(lb) $F_{max} = \chi_{i_{max}} F_S$	F_{max}		lb.
(8) Calculate inflation time, t_f(sec) $t_f = t_o \left(\frac{t_f}{t_o}\right)$	t_f		Sec.

DISTRIBUTION

	Copies
Commander Naval Air Systems Command Attn: Library	4
AIR-931H (F. Terry Thomasson) Technology Manager Crew Station & Life Support Systems (JP#1-Rm 424)	2
Department of the Navy Washington, DC 20361	
Commander Naval Sea Systems Command Attn: Library Washington, DC 20362	4
Commanding Officer Naval Personnel Research and Development Center Attn: Library Washington, DC 20007	2
Office of Naval Research Attn: Library Washington, DC 20360	4
Office of Naval Research Attn: Fluid Dynamics Branch	2
Structural Mechanics Branch	2
800 N. Quincy St. Arlington, VA 22217	

	Copies
Director Naval Research Laboratory Attn: Code 2027	
Library, Code 2029 (ONRL)	2
Washington, DC 20375	
U.S. Naval Academy Attn: Library Annapolis, MD 21402	2
Superintendent U.S. Naval Postgraduate School Attn: Library (Code 0384) Monterey, CA 93940	2
Commander Naval Air Development Center Attn: Library	2
Dr. Norman Warner	1
Kenneth Greene	1
William B. Shope	1
David N. DeSimone	1
Louis A. Daulerio	1
Thomas J. Popp	1
Maria C. Hura	1
Warminster, PA 18974	
Commanding Officer Naval Weapons Support Center Attn: Library	2
Mark T. Little	1
Crane, IN 47522	

DISTRIBUTION (Cont.)

	Copies
Commander Naval Ship Research and Development Center Attn: Library Washington, DC 20007	2
Commander Pacific Missile Test Center Attn: Technical Library, Code N0322 Point Mugu, CA 93041	2
Director Marine Corps Development and Education Command Development Center Attn: Library Quantico, VA 22134	2
Marine Corps Liaison Officer U.S. Army Natick Laboratories Natick, MA 01760	2
Commanding General U.S. Army Mobility Equipment Research and Development Center Attn: Technical Document Center Fort Belvoir, VA 22660	2
Commanding General U.S. Army Munitions Command Attn Technical Library Stanley D. Kahn Dover, NJ 07801	2 1
Commanding General U.S. Army Weapons Command Attn: Technical Library Research and Development Directorate Rock Island, IL 61201	2
Commanding General U.S. Army ARDEC Attn: Library Walt Koenig, SMCAR-AET-A Roy W. Kline, SMCAR-AET-A Dover, NJ 07801	2 1 1
Army Research and Development Laboratories Aberdeen Proving Ground Attn: Technical Library, Bldg. 313 Aberdeen, MD 21005	2
Commanding General Edgewood Arsenal Headquarters Attn: Library Aero Research Group Aberdeen Proving Ground Aberdeen, MD 21005	2
Commanding General Harry Diamond Laboratories Attn: Technical Library 2800 Powder Mill Road Adelphi, MD 20783	2

DISTRIBUTION (Cont.)

	Copies
U.S. Army Ballistic Research Laboratories Attn: Technical Library Aberdeen Proving Ground Aberdeen, MD 21005	2
Commanding General U.S. Army Foreign Science and Technoloy Center Attn: Technical Library 220 Seventh Street, NE Federal Building Charlottesville, VA 22312	2
Commanding General U.S. Army Materiel Command Attn: Library Washington, DC 20315	2
Commanding General U.S. Army Test and Evaluation Command Attn: Library Aberdeen Proving Ground Aberdeen, MD 21005	2
Commanding General U.S. Army Combat Developments Command Attn: Library Fort Belvoir, VA 22060	2
Commanding General U.S. Army Combat Developments Command Attn: Technical Library Carlisle Barracks, PA 17013	2
Commanding General U.S. Army Materiel Laboratories Attn: Technical Library Fort Eustis, VA 23604	2
U.S. Army Air Mobility R&D Laboratory Eustis Directorate Attn; Systems and Equipment Division Fort Eustis, VA 23604	2
President U.S. Army Airborne Communications and Electronic Board Fort Bragg, NC 28307	2
Commanding General Frankford Arsenal Attn: Technical Library Bridge and Tacony Streets Philadelphia, PA 19137	2
Commanding General U.S. Missile Command Redstone Scientific Information Center Attn: Library Redstone Arsenal, AL 358091	2
U.S. Army Natick Laboratories Liaison Office Attn: Library Aeronautical Systems Division Wright Patterson AFB, OH 45433	2

DISTRIBUTION (Cont.)

	Copies
Office of the Chief of Research and Development Department of the Army Attn: Library Washington, DC 20310	2
U.S. Army Advanced Material Concepts Agency Department of the Army Attn: Library Washington, DC 20315	2
Director U.S. Army Mobility R&D Laboratory AMES Research Center Attn: Library Moffett Field, CA 94035	2
Commandant Quartermaster School Airborne Department Attn: Library Fort Lee, VA 23801	2
U.S. Army Standardization Group, UK Attn: Research/General Material Representative Box 65 FPO, NY 09510	2
Commanding Officer McCallan AFB Attn: Library SA-ALC/MMIR McCallan AFB, CA 95652	2
Arnold Engineering Development Center (ARO, Inc.) Attn: Library/Documents Arnold Air Force Sation, TN 37389	2
NASA Lewis Research Center Attn: Library, Mail Stop 60-3 21000 Brookpark Road Cleveland, OH 44135	1
NASA John F. Kennedy Space Center Attn: Library, Code IS-CAS-42B Kennedy Space Center, FL 32899	1
NASA Manned Spacecraft Center Attn: Library, Code BM6 2101 Webster Seabrook Road Houston, TX 77058	1
NASA Marshall Space Flight Center Attn: Library Huntsville, AL 25812	1
NASA Goddard Space Flight Center Wallops Island Flight Facility Attn: Library Mr. Mendle Silbert Mr. Earl B. Jackson, Code 841.2 Mr. Dave Moltedo, Code 841.2 Mr. Anel Flores Wallops Island, VA 23337	2 2 1 1 1
National Aeronautics and Space Administration Attn: Library Headquarters, MTG 400 Maryland Avenue, SW Washington, DC 20456	2

DISTRIBUTION (Cont.)

	Copies
Defense Advanced Research Projects Agency Attn: Technical Library 1400 Wilson Boulevard Arlington, VA 22209	2
Director Defense Research and Engineering Attn: Library (Technical) The Pentagon Washington, DC 20301	2
Director of Defense Research and Engineering Department of Defense Washington, DC 20315	2
Defense Technical Information Center Cameron Station Alexandria, VA 22314	12
Library of Congress Attn: Gift and Exchange Division Washington, DC 20540	4
University of Minnesota Dept. of Aerospace Engineering Attn: Dr. W. L. Garrard Minneapolis, MN 55455	2

	Copies
Sandia National Laboratories Attn: Code 1632	2
Library	2
Dr. Dean Wolf	1
Dr. Carl Peterson	10
R. Kurt Baca	1
Ira T. Holt	1
Donald W. Johnson	1
James W. Purvis	1
Harold E. Widdows	1
Albuquerque, NM 87185	
Applied Physics Laboratory The Johns Hopkins University Attn: Document Librarian Johns Hopkins Road Laurel, MD 20810	2
National Academy of Sciences National Research Council Committee on Undersea Warfare Attn: Library 2101 Constitution Ave., N.W. Washington, DC 20418	2
Sandia Corporation Livermore Laboratory Attn: Technical Reference Library P.O. Box 969 Livermore, CA 9455	2
Lockheed Missiles and Space Co. Attn: Mr. K. French P.O. Box 504 Sunnyvale, CA 94086	1

DISTRIBUTION (Cont.)

Copies

Rockwell International Corporation Space and Information Systems Div. Attn: Technical Information Center 12214 S. Lakewood Boulevard Downey, CA 90241	2
Pennsylvania State University Applied Research Laboratory Attn: Library P.O. Box 30 State College, PA 16801	2
Honeywell, Incorporated Attn: M. S. Sopczak 600 Second Street N. Hopkins, MN 55343	1
National Bureau of Standards Attn: Library Washington, DC 20234	2
Internal Distribution:	
U13 (C. J. Diehlmann)	1
U13 (W. P. Ludtke)	35
U13 (J. F. McNelia)	1
U13 (D. W. Fiske)	1
U13 (J. Murphy)	1
U13 (M. L. Fender)	1
U13 (R. L. Pense)	1
U13 (M. L. Lama)	1
U43 (J. Rosenberg)	1
E231	2
E232	15
E31 (GIDEP)	1
C72W	1